Forschungszentrum Karlsruhe

in der Helmholtz-Gemeinschaft

Wissenschaftliche Berichte

FZKA 6852
SAM-ECOSTAR-D44

Melt Cooling by Bottom Flooding: The Experiment CometPC-H3

CONTRACT FIKS-CT1999-00003

EX-VESSEL CORE MELT STABILIZATION RESEARCH

H. Alsmeyer, T. Cron, G. Merkel, S. Schmidt-Stiefel, W. Tromm, T. Wenz

Institut für Kern- und Energietechnik
Programm Nukleare Sicherheitsforschung

Forschungszentrum Karlsruhe GmbH, Karlsruhe
2003

Acknowledgment

This work was partly funded by the European Commission in the Fifth Framework Programme under the ECOSTAR Contract FIKS-CT1999-00003.

Impressum der Print-Ausgabe:

Als Manuskript gedruckt

Forschungszentrum Karlsruhe GmbH
Postfach 3640, 76021 Karlsruhe

Mitglied der Hermann von Helmholtz-Gemeinschaft
Deutscher Forschungszentren (HGF)

ISSN 0947-8620

Abstract

The CometPC-H3 experiment was performed to investigate melt cooling by water addition to the bottom of the melt. The experiment was performed with a melt mass of 800 kg, 50 % metal and 50 % oxide, and 300 kW typical decay heat were simulated in the melt. As this was the first experiment after repair of the induction coil, attention was given to avoid overload of the induction coil and to keep the inductor voltage below critical values. Therefore, the height of the sacrificial concrete layer was reduced to 5 cm only, and the height of the porous concrete layers was also minimized to have a small distance and good coupling between heated melt and induction coil.

After quite homogeneous erosion of the upper sacrificial concrete layer, passive bottom flooding started from the porous concrete after 220 s with 1.3 liter water/s. The melt was safely stopped, arrested and cooled. The porous, water filled concrete was only slightly attacked by the hot melt in the upper 25 mm of one sector of the coolant device. The peak cooling rate in the early contact phase of coolant water and melt was 4 MW/m^2, and exceeded the decay heat by one order of magnitude. The cooling rate remarkably dropped, when the melt was covered by the penetrating water and a surface crust was formed. Volcanic eruptions from the melt during the solidification process were observed from 360 - 510 s and created a volcanic dome some 25 cm high, but had only minor effect on the generation of a porous structure, as the expelled melt solidified mostly with low porosity.

Unfortunately, decay heat simulation in the melt was interrupted at 720 s by an incorrect safety signal, which excluded further investigation of the long term cooling processes. At that time, the melt was massively flooded by a layer of water, about 80 cm thick, and coolant water inflow was still 1 l/s. The melt had reached a stable situation: Downward erosion was stopped by the cooling process from the water filled, porous concrete layer. Top and bottom crusts had formed, and included the bulk of the melt, which at this stage was still in the liquid state. Further cool down of the melt continued slowly over the next 40 min. Post test analysis showed, that the porosity of the melt is lower than in previous tests, and most of the coolant steam/water flow passes through one dominant flow channel at the base of the volcano. The interface of the porous concrete layer was only slightly attacked locally. The remaining 75 mm of porous concrete underneath are completely intact as always cooled by the presence of the flooding water.

In summary, the experiment has demonstrated that the CometPC cooling concept is able to stop and to cool the melt, although the expected porosity formation of the majority of the melt did not prevail in the present experiment. Under this aspect, the porous, water filled concrete layer has proven its reliability to stop the melt. On the other side, volcanic melt eruptions which occurred during a limited period of the test, did not improve the coolability significantly, as no major new porosity was created.

Kühlung der Schmelze durch Flutung von unten: das Experiment CometPC-H3

Zusammenfassung

Das Experiment CometPC-H3 wurde durchgeführt, um die Kühlung einer Schmelze durch Wasserzutritt von unten zu untersuchen. Das Experiment wurde mit einer Schmelzenmenge von 800 kg ausgeführt, die einen Anteil von 50 % Metall und 50 % Oxid aufwies, und in der typisch 300 kW Nachwärmeleistung simuliert wurde. Da dies das erste Experiment nach Reparatur der Induktionsspule war, sollte eine Überlastung der Induktionsspule vermieden und eine bestimmte niedrige Induktorspannung nicht überschritten werden. Dazu war die Höhe der Beton-Opferschicht auf nur 5 cm reduziert worden. Gleichzeitig wurde die Höhe der porösen, wasserführenden Betonschicht minimiert, um einen möglichst geringen Abstand und damit gute Ankopplung zwischen Induktionsspule und Schmelze zu erzielen.

Nach einer relativ gleichmäßigen Erosion der oberen Betonopferschicht begann nach 220 s die passive Flutung von unten durch Wasseraustritt aus der porösen Betonschicht mit 1,3 Litern/s. Dadurch wurde die Schmelze sicher gestoppt und gekühlt. Die poröse, wasserführende Betonschicht wurde nur in den oberen 25 mm lokal leicht angegriffen. Die maximale Kühlrate in der ersten Kühlphase lag bei 4 MW/m^2 und übertraf die Nachwärmeleistung um eine Größenordnung. Die Kühlrate nahm stark ab, nachdem die Schmelze von dem von unten eindringenden Wasser bedeckt war und eine Oberflächenkruste ausgebildet hatte. Vulkanische Eruptionen von Schmelze traten zwischen 360 und 510 s auf und bauten einen Vulkankegel von etwa 25 cm Höhe auf. Dies trug jedoch nur wenig zur Erzeugung einer porösen, gut kühlbaren Struktur bei, da die ausgetriebene Schmelze überwiegend als kompaktes Gebilde erstarrte.

Leider wurde die Nachwärmesimulation in der Schmelze nach 720 s durch ein fehlerhaftes Sicherheitssignal unterbrochen, was eine weitere Untersuchung der Langzeitkühlung verhinderte. Zu diesem Zeitpunkt war die Schmelze bereits durch eine 80 cm hohe Wasserschicht abgedeckt, und der Kühlwasserzustrom betrug noch 1 l/s. Die Schmelze hatte die folgende stabile Form angenommen: Die Erosion nach unten war durch die Kühlung des wasserführenden Porösbetons gestoppt. Oben und unten hatten sich stabile Krusten ausgebildet, die die noch flüssige Schmelze in ihrem Inneren einschloss. Die weitere Abkühlung der Schmelze vollzog sich über einen Zeitraum von 40 Minuten. Die Nachuntersuchungen zeigten, dass die Porosität der Schmelze geringer ist als in früheren Experimenten, und der Kühlwasserstrom des Wasser-Dampfgemischs sich auf einen Strömungskanal am Fuß des Vulkankegels konzentriert. Die Oberfläche der porösen Betonschicht wurde nur geringfügig angegriffen. Die untenliegenden 75 mm der Porösschicht sind vollständig intakt, da sie stets von dem einströmenden Kühlwasser gekühlt wurden.

Das Experiment hat gezeigt, dass das CometPC-Kühlkonzept in der Lage ist, die Schmelze zu stoppen und sicher zu kühlen, obwohl im vorliegenden Experiment die Schmelze nicht in poröser Form erstarrte. Die poröse, wasserführende Betonschicht hat damit ihre Stabilität gegen Schmelzeangriff unter erschwerten Bedingungen nachgewiesen. Andererseits haben vulkanische Eruptionen von Schmelze, die über einen beschränkten Zeitraum auftraten, nicht wesentlich zur Verbesserung der Kühlbarkeit beigetragen, da sie kaum neue poröse Strukturen entstehen ließen.

CONTENTS

1. Introduction

1.1 Background

Ex-vessel melt cooling is one of the demanding challenges which is essential to stabilize and terminate a core melt accident if the melt should penetrate the reactor pressure vessel. Resolving the coolability issue does not only require the removal of the sensible and the latent heat of the corium, but also of the fission product decay heat, which is a long lasting source of internal heat generation. Different options of direct contact of melt and coolant water are considered in various research institutions to resolve the coolability issue. Such investigations are also part of the ECOSTAR programme.

The COMET core cooling concept for ex-vessel melt cooling is based on bottom flooding: After erosion of a sacrificial concrete layer, the melt is passively flooded from the bottom by passive injection of coolant water. The water is forced up through the melt, the resulting evaporation process of the coolant water breaks up the melt and creates a porous, permeable structure of the melt from which the heat is easily extracted. Therefore, the porous melt solidifies within less than one hour typical and is permanently flooded by water.

The actual variant of the COMET cooling concept uses a layer of porous, water filled concrete from which the water is injected to the bottom of the melt after erosion of the sacrificial concrete layer atop. This variant, called CometPC concept (= Comet Porous Concrete), is presently investigated in large-scale experiments with respect to its efficacy and robustness.

The present report describes the first of the 3 experiments CometPC-H3 through H5, which have been performed as contributions to the ECOSTAR contract, which is partly funded by the European Commission.

1.2 Objectives

The CometPC-H3 experiment is designed as a large-scale test with a metal plus oxide melt that simulates the corium melt. The high initial temperature of the melt together with the simulation of the nuclear decay heat throughout the test allows an adequate representation of the corium melt. Simulation of the decay heat is necessary to allow the study of short and long-term heat transfer processes from the melt and to investigate reliable arrest of the melt. Exclusion of major basement erosion during ongoing release of nuclear decay heat is necessary to maintain containment integrity in a core melt accident.

Two preceding tests had shown that specific design options must be taken to supply sufficient coolant water homogeneously to the bottom of the melt. An additional layer of ceramic tiles was introduced between sacrificial and porous concrete layers to exclude blockage of the porous concrete by the upper layer of sacrificial concrete, thus allowing the necessary permeation of water to the bottom of the melt. The second test had indeed confirmed a substantial improvement of homogeneous melt cooling. However, this test was prematurely terminated after 52 minutes during the

long term cooling phase because of an electrical short circuit of the induction coil, which supplies the required decay heat to the melt. After repair of the induction coil, which is under the actual, experimental conditions a critical element of the overall test facility, the new test CometPC-H3 was planned not to overload the coil. This is achieved by better inductive coupling of melt and induction coil, and requires a reduced height of the sacrificial concrete layer, which in the present experiment was 5 cm only instead of 10 cm before.

The present experiment CometPC-H3 is a 1-dimensional section of about 1 m diameter of the larger cooling device, which would be used in a reactor. The height of the simulated corium melt is 32 cm. The decay heat, which shall be supplied to the melt, corresponds to 450 kW/m^2. These experimental conditions are representative for a corium melt that is spread to a surface of about 100 m^2, and with this conditions the experiment is a 1 to 1 representation of all important heat transfer and cooling processes, from onset of concrete erosion over start of flooding and cooling to final melt solidification and long term heat removal.

2. SYSTEM DESCRIPTION

2.1 Main test parameters

Figure 1 shows the basic design of the cooling device, used in CometPC-H3.

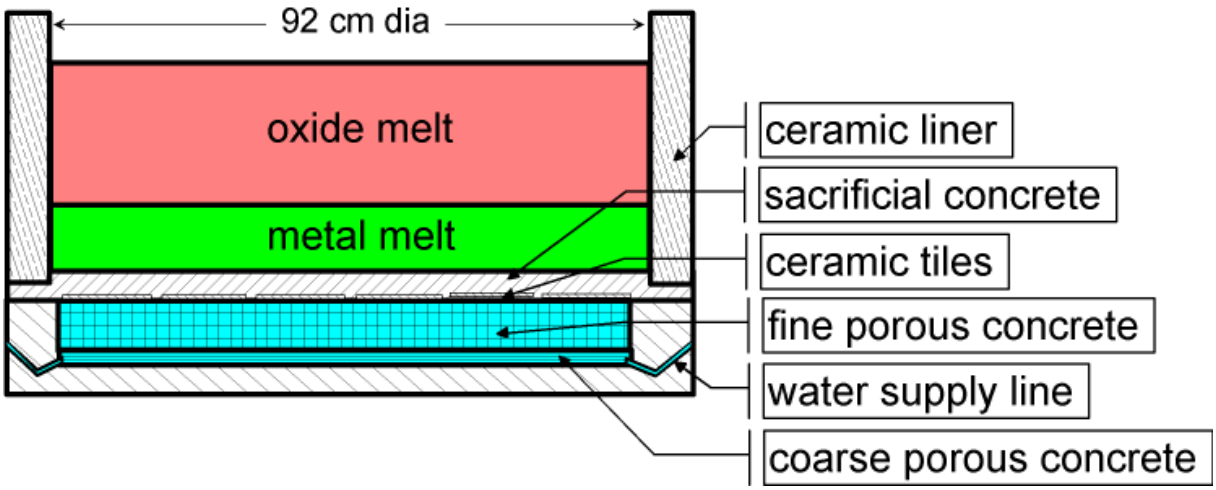

Figure 1: Schematic of the cooling device in CometPC-H3

The effective diameter of the horizontal coolant device is 92 cm, covered by 800 kg of melt. The height of the initial melt, without gases, is 32 cm in total, with 9.3 cm metal layer (400 kg) plus 22.5 cm oxide layer (400 kg) atop. The cooling device consists of 5 cm sacrificial concrete layer with ceramic tiles at the bottom, a 7 cm high layer of fine porous concrete and a 3 cm layer of coarse porous concrete. The porous concrete layers are flooded by coolant water from a water reservoir with a pressure, which is 0.1 bar above the hydrostatic pressure of the simulated corium

melt. The flow resistance of the upper porous concrete layer is designed to allow the appropriate coolant water flow into the melt, corresponding to an upper value of 3.6 litre/(m^2·s). Horizontal distribution of the water is achieved by the second, high porosity concrete layer underneath.

The lower boundary is formed by a support plate of conventional concrete. The cylindrical sidewalls are fabricated from refractory MgO ceramic rings, which favour a nearly 1-dimensinal experimental condition, as no sideward erosion does occur.

The cooling device is part of the large test assembly that is shown in Figure 2.

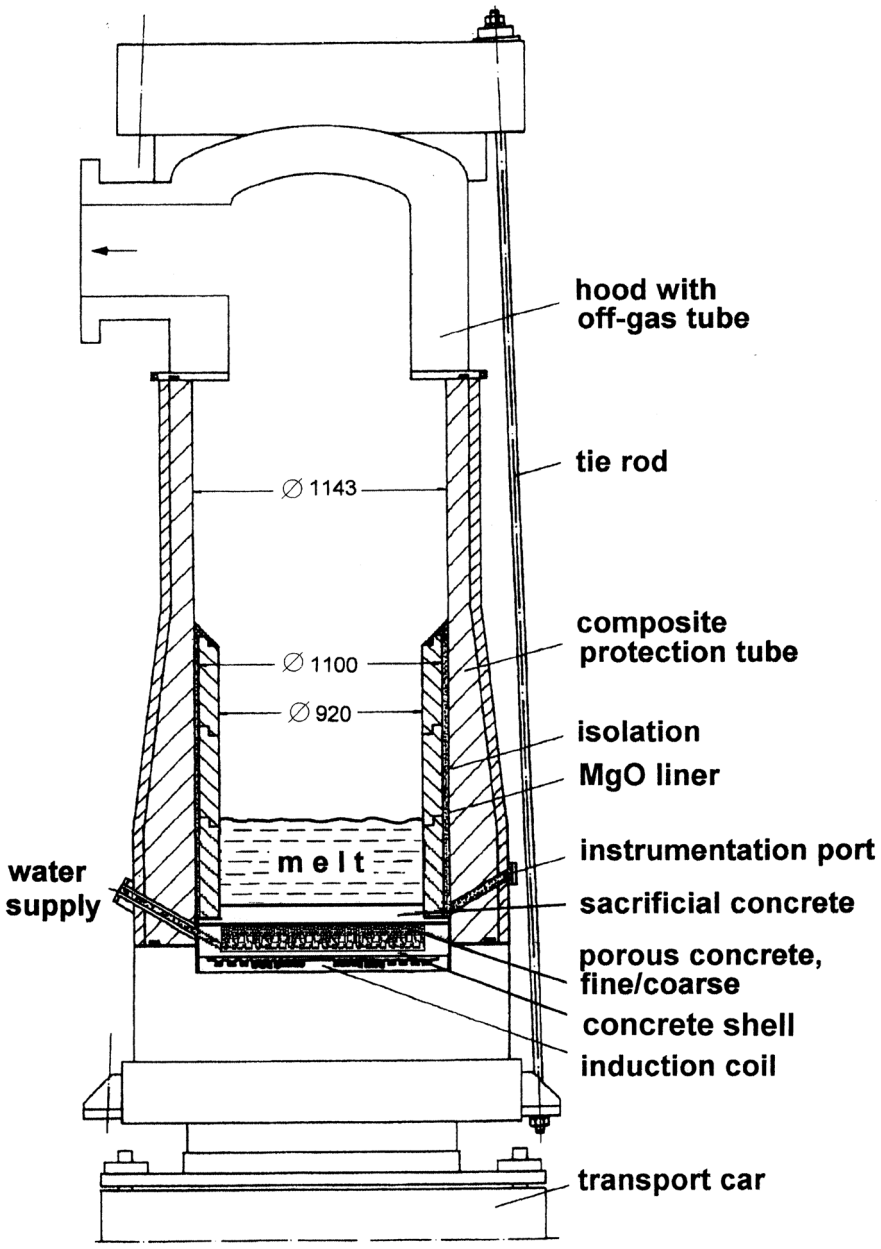

Figure 2: Schematic of CometPC-H3 Cooling Test

The simulated corium melt is generated externally by a thermite reaction with an initial temperature of about 1900°C and poured onto the cooling device through a lid in the hood of the crucible. This defines the experimental time zero, when the first phase of dry erosion of the sacrificial concrete layer begins. This phase is followed by passive onset of flooding, melt fragmentation, cooling and finally complete solidification. During all these processes, heating takes place through the induction coil, which is located under the bottom concrete shell of the coolant device.

All gases, which are generated during these processes, are collected in the free volume of the crucible, which is inerted by a defined argon cover gas flow, and feed through the off-gas tube to the open atmosphere. In this off-gas tube, the characteristics if the gas with respect to temperature, composition and flow rate are measured on-line.

The outer crucible is designed to withstand higher pressure pulses if they should occur. The test assembly is located on a transport car to allow installation and disassembly of the test rig. Figure 3 shows the test apparatus as part of the general installation.

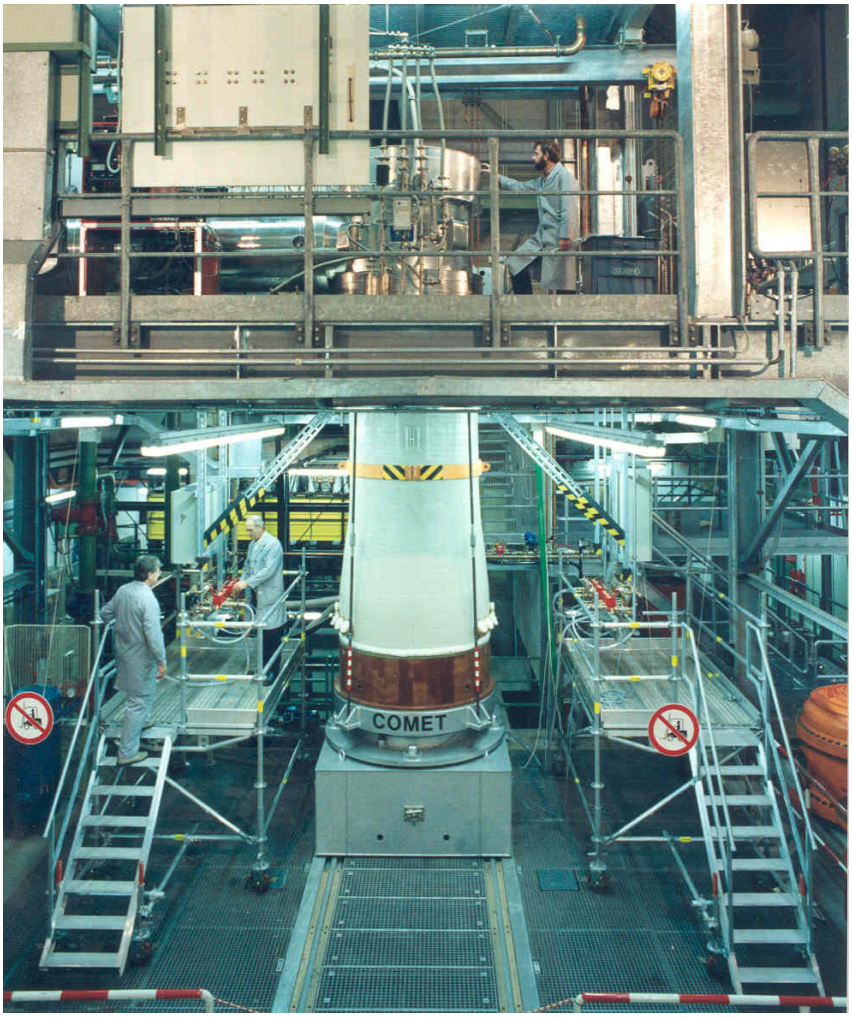

Figure 3: View of the COMET Facility

The next paragraphs describe important details of the test facility.

2.2 Melt and Melt Generation

The simulated corium melt is generated by a thermite reaction in an external thermite reaction vessel located above the test vessel. The basis for this reaction is a commercial thermite powder R70/SSH (Elektro -Thermit GmbH & Co KG, Essen, Germany), that produces liquid Al_2O_3 plus Fe by the strongly exothermic thermite reaction

$$Al + Fe_2O_3 = Al_2O_3 + 2\ Fe + h_{chem}\ .$$

To lower the freezing temperature and to increase the freezing range of the resulting oxide melt in accordance with the real corium melt, about 30 % of burned lime CaO is added to the thermite powder, which leads to the formation of a two component Al_2O_3 – CaO oxide melt mixture.

In addition, Ni pellets are mixed to the thermite powder, to produce a two component Fe/Ni – metal melt. The Ni fraction is necessary to influence the inductive coupling of the metal melt to the heater coil: For temperatures below the Curie temperature of 774°C, pure iron would change from paramagnetic to ferromagnetic behaviour. Consequently, inductive heating, which simulates the decay heat, would concentrate in the colder portions of the ferromagnetic iron “melt”, leading to a strongly non-homogeneous decay heating. The addition of 15 % Ni to the Fe melt reduces the transition to ferromagnetism to 400°C, and thus allows further induction heating of the solidifying metal melt.

The following Table 1 shows the composition of the thermite powder and the resulting melt composition.

Table 1: Composition of the thermite powder and of the resulting melts

Constituent	kg
Initial composition:	
Thermite powder R 70/SSH	618.2
CaO	216.4
Ni	60.0
total	894.6
Generated melt:	
Oxide: 56.2 % Al2O3 + 43.8 % CaO	494.6
Metal: 85.0 % Fe + 15.0 % Ni	400.0
total	894.6

To compensate for the high masses of CaO and Ni, the thermite powder is preheated to about 200°C by electrical heater rods in the thermite reaction vessel, before ignition of the thermite. The resulting temperature of the melt pour is 1900°C. The time between ignition and pour is 90 s. As thermite burn is completed after 25 s, the

residual time is sufficient that the metal phase segregates completely to the bottom of the reaction vessel, covered by the pure oxide melt.

All metal melt (400 kg) is poured through a lid in the hood of the test vessel, followed by 400 kg oxide melt, controlled by an on-line weighing system. The residual oxide melt is discharged to a slag container.

The height of the metal melt in the test vessel, without void by the percolating gases, is 93 mm, and 225 mm for the oxide melt, resulting in a total height of 320 mm. The calculated densities of the melts are 6470 kg/m^3 for the metal phase and 2670 kg/m^3 for the oxide phase. Therefore, the oxide phase is on top of the metal phase, as expected in the reactor situation after dilution of the oxide melt by eroded concrete.

2.3 Crucible and Cooling Device

The test crucible, as shown in Figure 2 and partly described in Paragraph 2.1, is equipped with the cooling device, the induction coil for decay heat simulation, water supply, and all necessary instrumentation. The crucible is gas tight, so that all gases, released during concrete erosion and during cooling of the melt, are collected in the free volume and transferred through the hood and the off-gas tube to the open atmosphere. Before start of the melt pour, the atmospheric gases are replaced by argon cover gas to exclude any burn in the crucible or off-gas tube.

At time zero, the 800 kg melt is poured into the crucible. The pour is completed after some 50 s. Subsequently, the lid is closed. Inductive heating by the induction coil supplies the required decay heat throughout the test.

The following elements are essential for the crucible and cooling device:

- The support structure, which includes the water-cooled induction coil, is located on the transport car. As all other components, which are close to the induction coil, the structure is fabricated from non-metallic materials. The upper free surface of the induction coil is covered by a 6 mm silicone foil, which protects the coil against any water that could be released during the cooling process atop. The induction coil is connected to the electrical induction circuit and to a specific water-cooling system.
- To minimise inductive losses, the cooling device is directly positioned on the silicone foil above the induction coil. This concept relies on the efficacy of bottom flooding and cooling, as the distance between hot melt and induction coil is only about 15 cm.
  The cooling device, as detailed in Figure 1, is described in Paragraph 2.1. The upper layer of sacrificial concrete is fabricated with aggregates of broken borosilicate glass with the following composition: SiO_2 62,5 %, B_2O_3 > 6 %, Al_2O_3 > 5 %, Na_2O 14,5 %, CaO 6 %, MgO 3,5 %, TiO_2 < 1 %, Fe_2O_3 < 1 %, K_2O >1 %, other impurities <0,5 %. This glass, when melted and mixed to the simulated or real corium melt, reduces its viscosity and thus favours the spreading process. In addition, the boron as strong neutron absorber eliminates criticality problems.
- Three cylindrical rings of MgO oxide, 920 mm inner diameter, 90 mm thick, form the radial confinement of the melt. As MgO is sufficiently stable, the melt can only

attack the structures below. The gap between the MgO rings and the protection tube is filled with dry quartz sand for thermal insulation.

- The composite protection tube is formed by an inner structure of refractory concrete, and an outer shell of gas tight, high temperature epoxy.
- The upper hood is a steel structure with inner ceramic liner. It is connected to the off-gas tube.
- 4 tie rods tighten upper and lower parts of the crucible, and maintain its integrity if inner mechanical loads should act on the structures.
- 4 redundant water supply lines are connected to the coolant device to supply the coolant water for bottom flooding.
- 2 instrumentation ports are used for thermocouple and glass fibre instrumentation of the cooling device

2.4 Water Supply

The coolant water for passive bottom flooding of the melt is supplied from a water tank, which is located about 2 m above the inner bottom surface of the cooling device. The effective overpressure of the coolant water, taking into account the hydrostatic pressure of the 32 cm high melt, is 0.1 bar, which is the specified overpressure for the actual test. The water level in the water tank is kept constant by level control and refill of fresh water from the building supply system. The temperature of the water is 20°C.

As the sacrificial concrete layer in the actual test is only 5 cm thick, this layer is not sufficiently watertight and requires a specific water management, to avoid water accumulation before pour of the melt. (Under normal conditions, the sacrificial layer would be 10 cm thick or more, and hence completely water tight.) For the actual test, the porous concrete layers are connected to the water tank 210 s after start of the melt pour. This avoids early migration of water, but allows onset of flooding if the sacrificial concrete layer is eroded.

The operator has several possibilities to modify the water flow if required during the course of the experiment. He can interrupt the bottom water flow and discharge the accumulated water into an external water tank. In addition, a spray system can be activated from the top of the crucible, which brings coolant water to the surface of the melt. These options are used after end of the experiment to unload the test vessel.

2.5 Off-gas System

The off-gas system, which is connected to the crucible hood, consists of a horizontal connecting tube, 1 m long, with a ceramic liner of 40 cm inner diameter, a vessel to retain any melt which could be ejected from the test vessel, and an 11 m long horizontal steel tube of 50 cm inner diameter, exhausting the gas flow to the atmosphere outside of the building.

The large flow diameter of the off-gas system excludes pressure build-up in the test vessel even for high gas rates. The off-gas system is preheated to 110 °C before and during the experiment to exclude condensation of steam. The end of the off-gas tube

is closed by a paper diaphragm, which allows argon inertisation before start of the test. The diaphragm is expelled by the first hot gases produced during pour of the melt. Off-gas analysis is performed by instrumentation located in the long off-gas tube.

At the end of the off-gas tube, a heater plug ignites the off-gas if the concentration of burnable gases is sufficient. A standing flame usually characterizes the first phase of dry concrete erosion.

2.6 Decay Heat Simulation

Decay heat is simulated in the melt by induction heating which couples to the metallic fraction of the melt. The horizontal induction coil, located under the cooling insert, forms the resonance circuit together with a set of 27 large high voltage capacitors, driven by a 1 kHz power supply.

The maximum inductor voltage is 2600 V, the maximum current 12000 A. The rated upper heating power for a non-magnetic (paramagnetic) melt is 400 kW.

The heating power deposited in the melt is determined online by the measured actual total power from which the losses by ohmic resistance and by the electromagnetic stray field are subtracted. These losses were determined in separate system tests, depending on voltage and currents of the induction circuit. In addition, a complete balance of all electric cooling circuits confirms the validity of this approach.

During the experiment, the inductive power is adjusted by control of the inductor voltage. This is performed manually by the operator, based on the displayed actual power history. The net heating power strongly varies with the coupling efficiency between induction coil and metal melt. Three reasons influence the electromagnetic coupling: (1) Agitation and the variation of void in the melt: For higher void, the efficiency of coupling is reduced. Strong high frequency power oscillations are characteristic for the early MCCI processes and during onset of bottom flooding. Solidification of the melt, in whatever structure, leads to more stable coupling. (2) The reduced distance between melt and induction coil, which is a consequence of concrete erosion, improves the coupling. (3) The electrical properties of the metal melt change with temperature. The most important property for the actual melt is the magnetic permeability, which for the Fe-Ni melt strongly increases below the Curie temperature, i. e. below 400°C. This will occur after solidification and further quenching of the “melt” or parts of the melt, resulting in a higher efficiency of heating.

For the present test, the induction coil is started 4 minutes before pour of the melt. The decay power will be increased from about 150 kW at start of the test to 300 kW after onset of cooling. The power limitation in the first phase to 150 kW is expected to avoid pronounced local, inhomogeneous erosion of the sacrificial concrete.

2.7 Instrumentation and Data Acquisition

The Comet facility is equipped with a multitude of instrumentation to monitor and control the experiment and to collect data for subsequent evaluation. Besides

registration on chart recorders and printers, all data are stored and displayed on a PC data acquisition system.

More than 100 measurement signals are collected to characterise the following information:

1. Electrical induction heating: Gross power, net power, various voltages and currents, inductor frequency, control temperatures and coolant flows
2. Generation and pour of the thermite melt: Mass of melt in the thermite reaction vessel, temperature of melt during pour, signals to control the pour
3. CometPC cooling device: Temperature and erosion profile of the sacrificial concrete layer and of the porous concrete layers, temperature in the structures nearby, glass fibre instrumentation as ultimate safety signal in case of extreme melt penetration
4. Coolant flow to the cooling device: Water flow rate, water pressure (including possible pressure pulses), height of water level during flooding
5. Upper crucible hood: Temperatures and pressures in the gas room, control and rate of the argon cover gas flow
6. Off-gas system: Gas flow, temperature, and pressure; gas composition by on-line quadrupole mass spectrometry and aerosol density by transmission of laser beam
7. Control signals and conditions of the experimental hall

The temperature of the melt during the interaction and cooling phase cannot be measured because of the chemically aggressive melt. In previous experiments, the lifetime even of PtRh10-Pt (type S) thermocouples was not sufficient to detect a reliable temperature of the melt.

Several video systems are used to observe the experiment, including two video installations, which are directed from the crucible hood onto the surface of the melt. These systems are especially useful to observe all processes, which are related to melt fragmentation and cooling.

3. Experiment Results

3.1 Test Procedure

The conduct of the experiment was planned as given in Table 2. The time t = 0 is defined by start of the melt pour. Deviation from the test plan occurred because of an erroneous control signal that interrupted power supply and further decay heat simulation at 720 s and excluded the investigation of long-term cooling. The reason for the erroneous signal was slow heat-up of a bundle of thermocouples lines outside of the cooling insert by the electromagnetic stray field of the induction coil. Because of their elevated temperatures, the thermocouple lines interrupted an optical glass fibre instrumentation outside of the crucible. The loss of the glass fibre signal automatically initiated shut-down of the power supply, assuming an extreme, but incorrect downward or sideward propagation of the melt.

Table 2: Planned conduct of the CometPC-H3 experiment

Time, s	Event
until –240	Facility prepared, argon inertisation completed, induction coil operating
-90	Ignition of thermite powder, allow separation of metal and oxide phases
0	Start of melt pour (27 s), onset of erosion of sacrificial concrete layer, continuous decay heating with about 150 kW
210	Connect water supply to the porous layers of CometPC coolant device
about 300	Onset of passive flooding expected after erosion of sacrificial layer; operator shall increase decay heat to 300 kW until end of heated test. Observation of melt fragmentation, cooling, and solidification
about 1800	Complete melt solidification expected, further heating with 300 kW to observe stability of long-term cooling over further 1800 s
about 3600	End of heated test, decay power of
post test	Cool down and release of water from flooded and solidified melt, inspection and conservation of test vessel for further dismantling

The realized experimental conduct is provided in Table 3. After completion of the test preparation, the thermite powder was ignited 90 s before start of the melt pour.

Table 3: Realized conduct of the CometPC-H3 experiment

Time, s	Event
until -90	Test preparation as planned, induction coil operating
-90	Ignition of thermite powder, thermite burn complete after 25 s, separation of metal and lighter oxide phases
0 → 210	Start of melt pour: 800 kg metal + oxide melt with 1900°C, completed after 49 s. Onset of dry erosion of sacrificial concrete layer, average downward erosion rate 0.17 mm/s. Simulated decay heat from 100 to 160 kW. No hydrogen flame at end of off-gas line throughout the test.
210	Water supply connected to porous layers of coolant device
230	Passive onset of bottom flooding with 1.3 l/s. High flooding rate indicates sufficient opening of flow channels from the porous concrete layer. Melt strongly agitated by strong steam flow, melt droplets of a few cm only ejected from melt surface. Only mild interaction of melt and water, no pressure spikes. Strong cooling by complete water evaporation, peak cooling rate 3 MW (= 4.5 MW/m²). Heating power increased by operator to reach planned 300 kW, but strong variations in efficiency of induction heating.
280	Melt surface mostly flooded by boiling water, fast reduction of the high cooling rate. Aerosol release ended.
300 →360	Melt surface mostly dark (one hot spot) and completely covered by water. Passive flooding continues with 1.4 l/s. Hot particles ejected under water, driven by moderate volcanic eruptions through steam flow until 510 s.
430	Surface of melt dark (solid), boiling continues
450	Substantial increase of heating efficiency, probably caused by drop of metal temperature below 400°C (transition to ferromagnetism)
510	End of volcanic eruptions. Volcano, which formed, is about 25 cm high (post test analysis). Fractions of central melt probably still liquid. Melt encrusted by top and bottom crusts.
680	Low temperatures in porous concrete layer indicate stable barrier, only one of five TCs at –5 mm failed, indicating very limited propagation and stop of melt into porous, water filled concrete layer.
720	End of induction heating by interruption through incorrect control signal (failure of glass fibre instrumentation outside of crucible)
post test	Coolant water flow continues, melt cooling and quenching completed over the next 40 minutes, accumulated coolant water drained out. Test vessel prepared for further analysis.

Figure 4 is the weight of the thermite reaction vessel, which shows the reaction period of the thermite (from –90 to –63 s) and the pour starting at time zero. Thermite burn was completed 27 s after the ignition (at - 63 s, indicated by the end of oscillations of the weighing system), which is the standard reaction time. The subsequent time of 63 s is sufficient to allow complete segregation of metal and oxide phases. Note, that the thermite weight has a constant offset of about 60 kg.

The pour of 800 kg melt, starting at time zero (definition of t = 0 s), is completed after 49 s. At that time, the remaining 90 kg oxide melt is transferred to the slag wagon. The crucible hood is closed upon completion of the pour after 93 s, so that all gases are directed through the off-gas line. During the pour of the melt, the weighing system shows untypical oscillations, which are probably caused by some residual material in the orifice of the reaction vessel, which obstructs free outflow of the melt, but which is finally removed at the end of the pouring process. Two different slopes characterise the weight reduction: The steeper slope is related to the release of the denser metal, and reduces to a more moderate slope, when the melt after release of 400 kg changes from metal to the lighter oxide. The intersection of the two slopes confirms the expected mass of the metal phase.

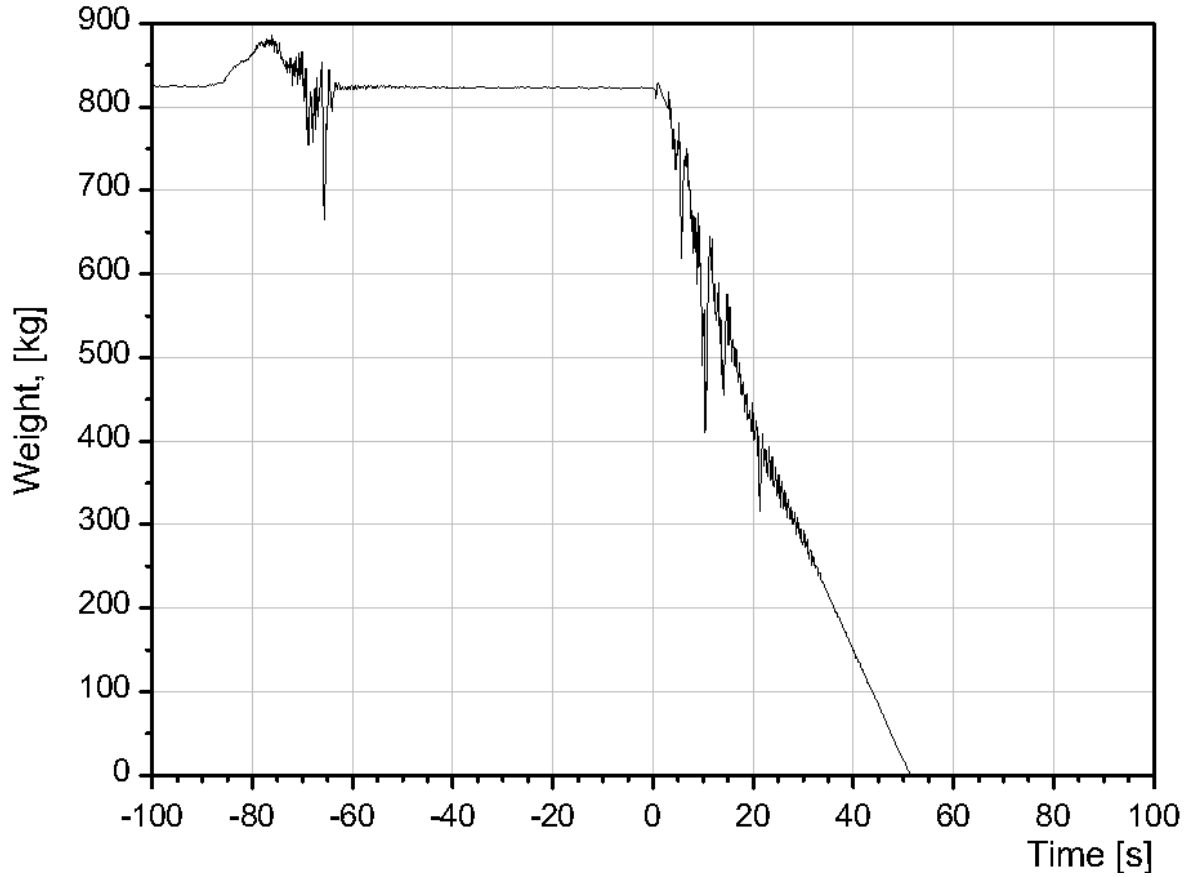

Figure 4: Weight of thermite vessel during thermite burn and melt release

The thermocouple, which was intended to measure the temperature of the melt in the spout, failed at 1750°C before reaching the final temperature. The temperature of the melt when poured to the test crucible, is expected to be 1900°C as measured in the analogous preceding tests.

The first phase of the experiment is characterized by the dry erosion of the upper 5 cm layer of sacrificial concrete. The melt is strongly agitated by the gases, predominantly steam, released from the decomposing concrete. The steam is partly reduced to hydrogen by chemical reaction/oxidation of the steel melt. The H_2 content in the off-gas is however so low, that the hydrogen being diluted with the argon cover gas is not ignited at the end of the off-gas line. In this early interaction phase, low density aerosols form, which allow only a diffuse surface of the melt to be observed during the first 160 s. Net induction heating is between 100 and 160 kW, strong variations in the efficiency of heating are correlated to the melt agitation. The erosion of the sacrificial concrete layer is relatively even and homogenous with an average erosion velocity of 0.17 mm/s. The temperature of the melt decreases, and melt agitation is moderate at 180 s, when thermocouples in the sacrificial concrete layer detect propagation 30 mm deep.

At 210 s, the valve is opened to connect the flooding water tank to the porous concrete layers in the coolant device. This establishes the necessary condition that bottom flooding can start passively when the sacrificial concrete layer is eroded.

At 230 s, the passive water addition from the bottom starts and immediately reaches 1.3 litre/s flow rate. The high steam flow from the evaporating coolant water produces strong, turbulent agitation of the melt, which at this moment still has a low viscosity and elevated temperature. The melt volume increases because of the high void from the evaporating water. A large number of melt droplets with typical dimensions up to 1 or 2 cm are ejected by the gas from all over the melt surface and rise several 10 cm into the free volume above the melt. This characterizes an effective fragmentation process. The high steam rate leads to a significant increase of the off-gas flow, and superheated steam escapes from the off-gas tube. It is interesting to note that the bottom flooding process does not produce strong pulsations of the melt, but a more continuous dispersion process. No energetic melt water interactions or steam explosion do occur. The intensity of the interaction decreases as the melt cools down, and the aerosol release declines to virtually zero.

At 280 s, the melt surface is mostly covered by a thin layer of boiling water that percolated through the melt. The bottom coolant water flow is unchanged with 1.3 l/s. However, the melt including its surface is still liquid and bright, and continuously agitated by the steam flow. The decay power in the melt increases to the planned 300 kW, but is still subject to major oscillations as heating efficiency varies from 30 to 50 %. The surface of the melt is mostly dark after 360 s with the exception of one hot spot which develops as the centre of moderate volcanic eruptions under water. Hot particles are ejected and settle or bond to the surface of the upper melt crust. This volcanism ends at 510 s and has built up an irregular rough cone about 25 cm high. At this time, the centre of the melt is still partly liquid as significant power oscillations still occur. The melt is encrusted between top and bottom crusts and internally cooled by percolating steam/water flow. Decay heating is continuing, and the continuous high efficiency of heating of 50 % indicates, that the solidified fraction of the steel melt is in the ferromagnetic state, that is below 400°C.

At 680 s, the constant temperatures in the porous concrete layer indicate stabilisation of the melt front. The maximum propagation of the melt into the upper porous, water filled concrete layer is –5 mm, as detected by one single thermocouple. In the porous concrete layer, all other thermocouples show temperatures below or close to 100°C,

i. e. the temperature is limited by the boiling water. The stability of the porous concrete layer is therefore maintained, and the melt is safely arrested. A small hydrogen rate is still detected in the off-gas, produced by chemical reaction of steam and iron. The water layer above the melt reaches the level 120 cm above the porous concrete. The rising water level reduces the effective overpressure of the coolant water and therefore the coolant water flow decreases to about 1 l/s.

At 720 s, decay heating is interrupted by a safety signal, which is generated by failure of one glass fibre instrumentation outside the crucible, as described above. This stops the heated period of the test in the phase, where the melt was safely stabilized and investigation of the long term stability was in progress.

The bottom flow of the coolant water continues. 40 minutes after start of the test, boiling from the solidified melt has come to an end. The accumulated water is then released from the crucible and the crucible is preserved for later analysis. The outer view of crucible and facility show that the installation is completely intact. Neither the hot melt nor the cooling progress had any influence on the outer structures.

3.2 Test Results

This section summarizes the principal measurements of the CometPC-H3 cooling test.

3.2.1 Simulated Decay Heat

Figures 5 through 7 show the characteristics of induction heating from start of melt pour (time 0) until 2000 s for the net power, the voltage supplied to the induction coil, and the efficiency of heating, which is defined as the net power to the melt divided by the total electric power delivered to the induction system. Heating efficiency is equivalent to the inductive coupling of the melt to the electromagnetic field.

The voltage of the induction coil is under control of the operator, who adjusts the voltage to achieve the net power input to the melt (decay power) according to the test plan. The operator uses on-line information about the total power and the net power to the melt.

At time zero, the induction coil is operated with 1.3 kV constant voltage, which is the expected voltage to heat the melt with about 150 kW. As the melt is poured into the crucible, the decay power rises to 190 kW within the first 20 s. The subsequent decrease of the net power to 100 kW is probably due to porosity formation in the steel melt and due to dispersal of some steel melt into the oxide melt, which reduces the efficiency of inductive coupling. These processes are influenced by the interplay of gas release from dry MCCI and the physical properties of the steel and oxide melts, especially by their viscosities and density ratios. A reduced release of concrete gases may be responsible for some increase of decay power until 120 s. At this time, the operator increases the inductor voltage to 1.45 kV to stabilize the decay power at 150 kW. This is, however, partly counterbalanced by a reduced heating efficiency, so that the decay power is near 140 kW.

Upon onset of bottom flooding after 230 s, the heating efficiency suddenly changes from about 30 to some 50 %, although the induction voltage remains nearly unchanged. This rises the simulated decay power to about 300 kW, which is the value, which is planned after start of flooding until end of the heated test phase. Subsequently, the operator tries to adjust the induction voltage to be in agreement with the planned net heating power of 300 kW. The high heating efficiency of 50 % between 230 and 300 s is unexpected. Afterwards, the efficiency declines to 30 %, which is the typical value for a high temperature melt. The operator's increase and slight decrease of the voltage brings the power above and near the planned 300 kW decay power level. At 500 s, the efficiency rises again close to 50 %. At this time, cool-down of the melt is proceeded: The water flow, entering from the bottom, is accumulating on top of the melt; its surface is quenched, and the volcanic eruptions are coming to an end; downward melt propagation is stopped, and the steel melt is partly solidified and below the Curie temperature. It is therefore the transition to ferromagnetism (below 400 °C) that brings the heating efficiency up to about 50 %. The maximum value of induction efficiency is determined after cool-down of the melt to room temperature after the test as 55 %.

At 720 s, the figures show stop of heating by the control signal. At 850, 920, and 1900 s the induction voltage shows a short peak, as the operator tries to restart the power supply, but without success.

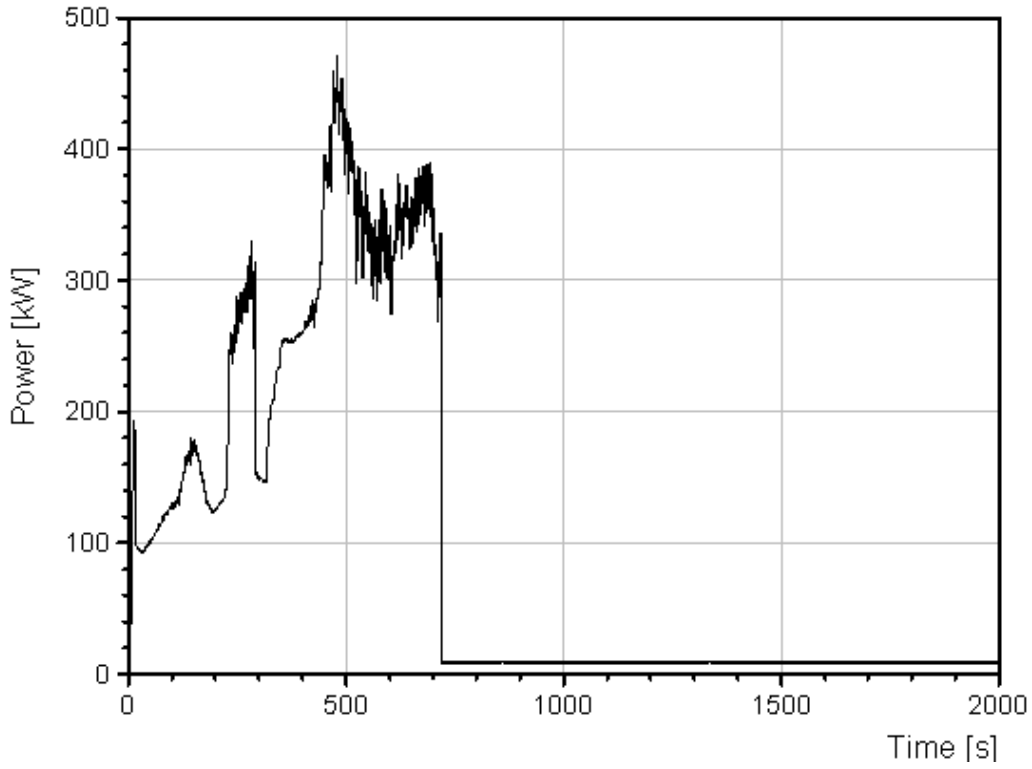

Figure 5: Simulated decay heat by induction heating of the melt (net power)

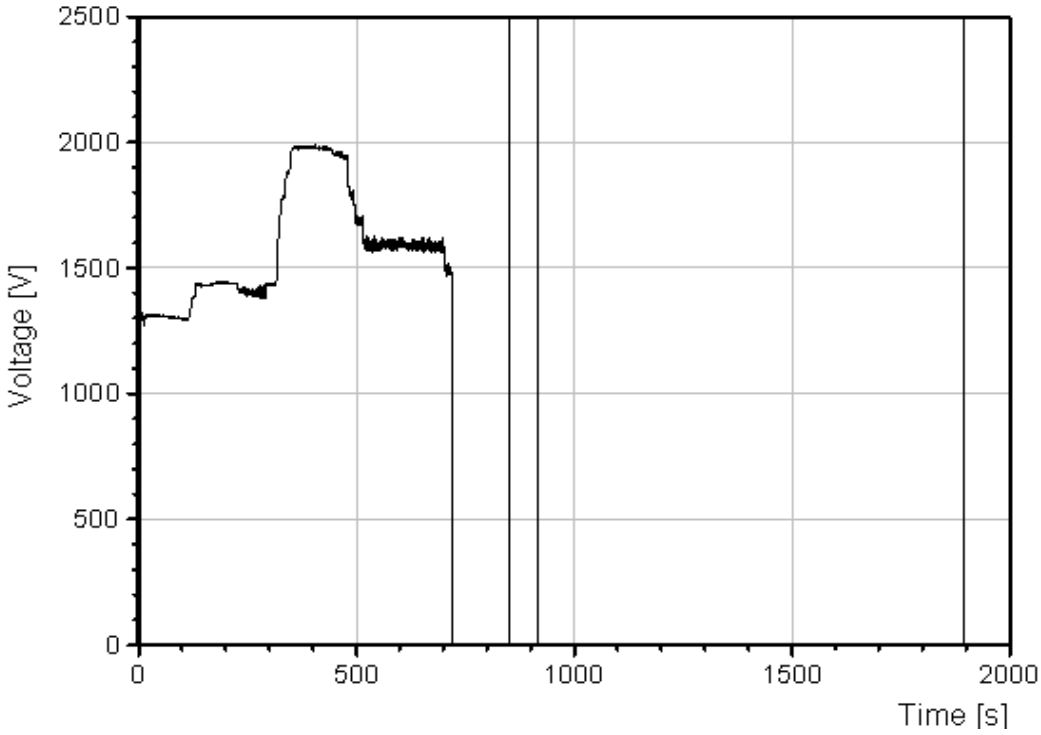

Figure 6: Voltage of induction coil

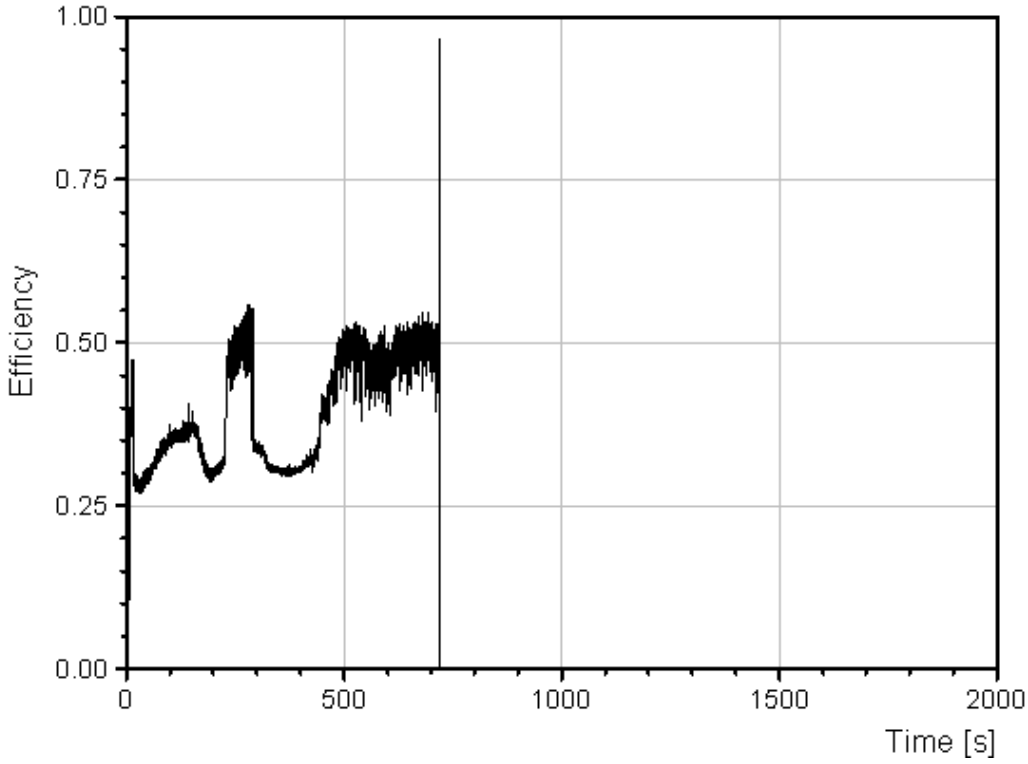

Figure 7: Efficiency of induction heating

3.2.2 Bottom Coolant Flow

Figures 8 through 10 show the coolant water flow to the bottom of the melt, the approximate water level in the crucible, and the water pressure in the supply lines, respectively.

Figure 8 clearly shows the onset of bottom flooding at 220 s, rising to 1.3 litres/s in the first cooling phase. In case of complete evaporation, this water flow could evacuate 3.4 MW, that is more than a factor 8 than generated by decay heat. The high coolant flow, compared with the maximal design value of 2.4 litres/s, indicates that the surface of the porous concrete layer is in wide parts permeable for the bottom water flow. At 300 s, a limited increase of the flow rate indicates a larger or additional flow path, which develops during the test. Thereafter, the flow rate monotonically decreases because of the continuous accumulation of water on top of the melt, which reduces the driving water pressure. The volcanic eruptions from 360 to 510 s have no effect on the overall water flow. At end of heating at 720 s, the inflow is 1.0 litre/s, further decreasing. The water flow plotted until 2000 s shows slight oscillations which result from control and refill of the water level in the supply tank.

Figure 9 gives an approximation of the water level in the crucible. This measurement is based on overflow or penetration of coolant water through the MgO rings and represents the actual water level in the isolating gap between MgO rings and inner protection tube. Consequently, the actual level in the crucible is indeed higher than the measured water level in Fig. 9, which nevertheless indicates the fast flooding of the melt.

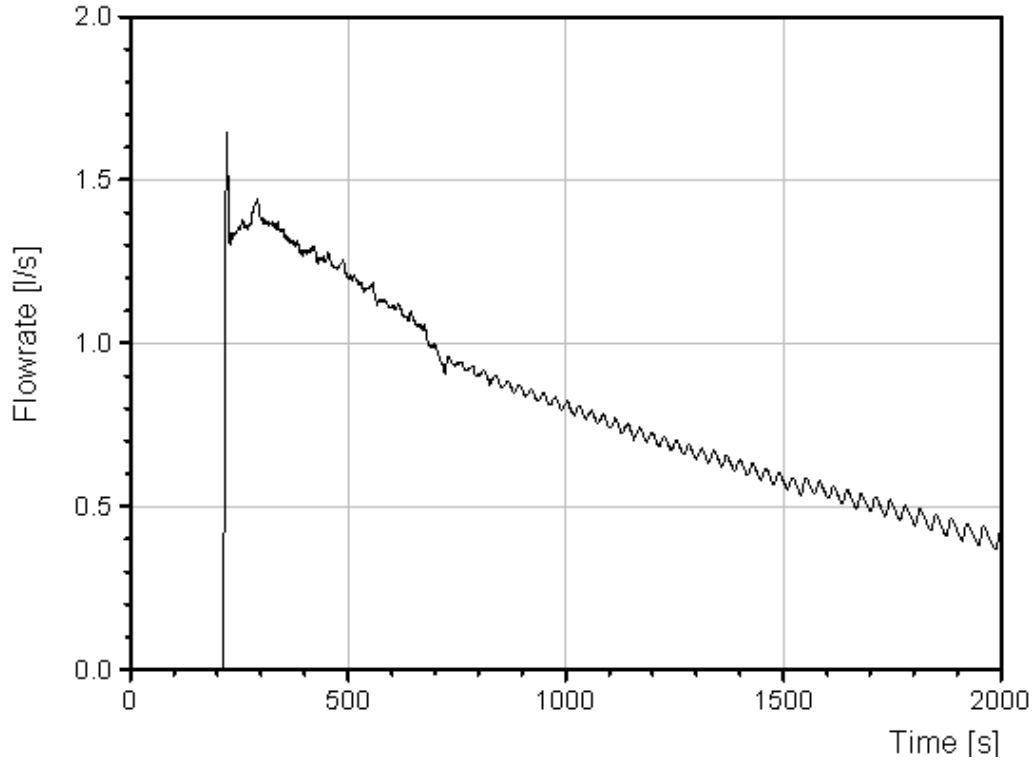

Figure 8: Bottom water flow to the melt

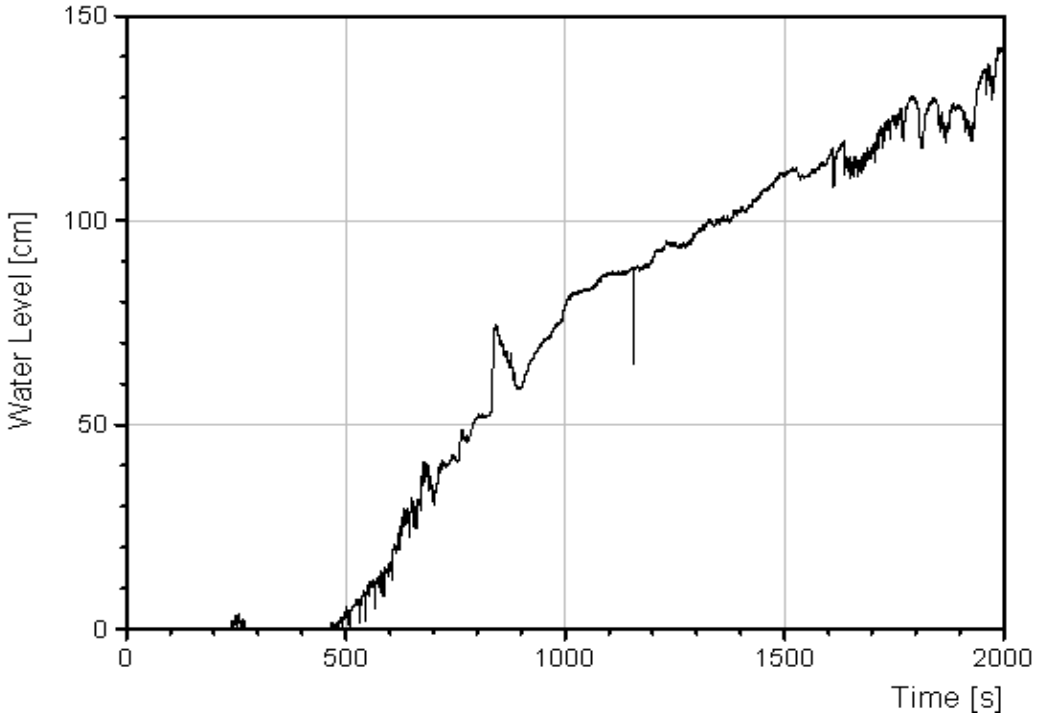

Figure 9: Approximate water level in crucible

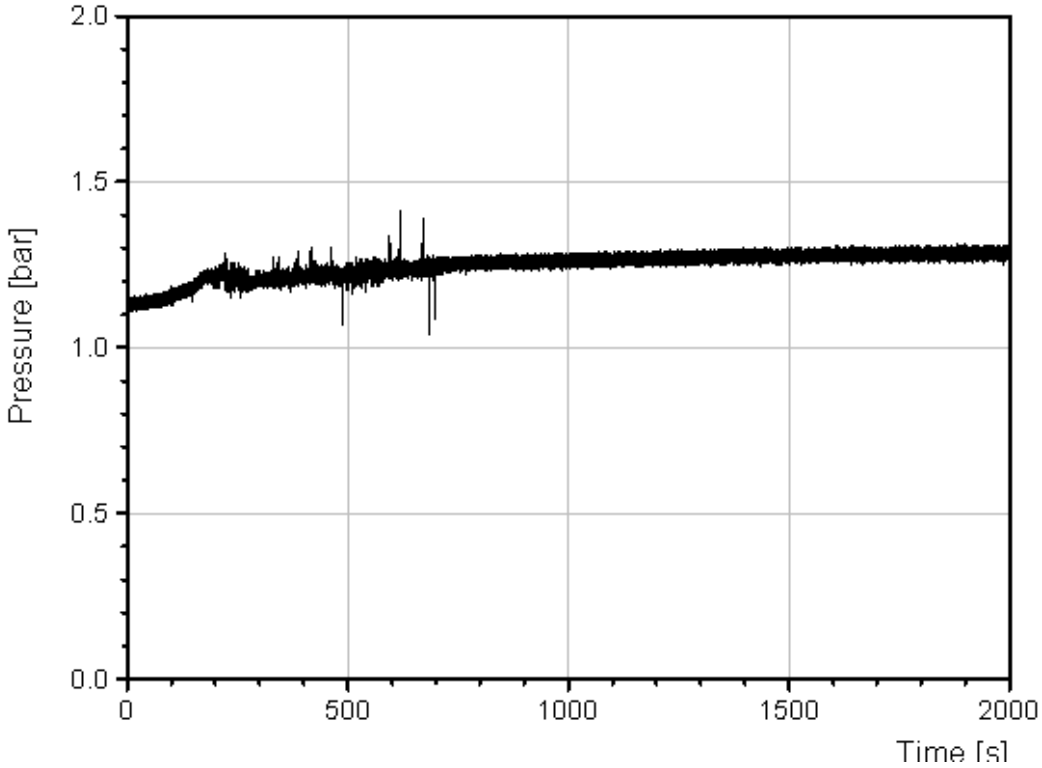

Figure 10: Coolant water pressure in supply lines

Figure 10 gives the absolute water pressure in the supply lines which corresponds to the pressure in the water filled porous concrete layer, connected at 210 s to the water supply tank. This results in a nearly constant overpressure of 0.1 bar over the hydrostatic pressure of the melt. Pressure variations are very small, and no major pressure increase is visible which could result from intense melt water interactions.

3.2.3 Heat removal by evaporation

With onset of melt cooling by bottom flooding, a large amount of steam is generated, which is released through the off-gas tube. In the off-gas tube, gas velocity and its temperature are measured simultaneously, which, after subtraction of the argon cover gas flow, and referred to the measured gas temperature in the hood of the crucible, allow calculation of the enthalpy in the steam flow. This is in good approximation the heat flux extracted from the melt by evaporation of the bottom coolant flow.

Fig. 11 gives the measured cooling power, which starts at 220 s and rises up to 3 MW for about 50 s. During this period, the injected water is evaporated completely. Then, the extracted power drops to about 500 MW at 320 s and then approaches the simulated decay power at 500 s. Subsequently, the gas temperature falls below 100°C, so that onset of condensation does not allow further determination of the evaporated enthalpy flux.

Figure 11: Power extracted by evaporation of coolant water

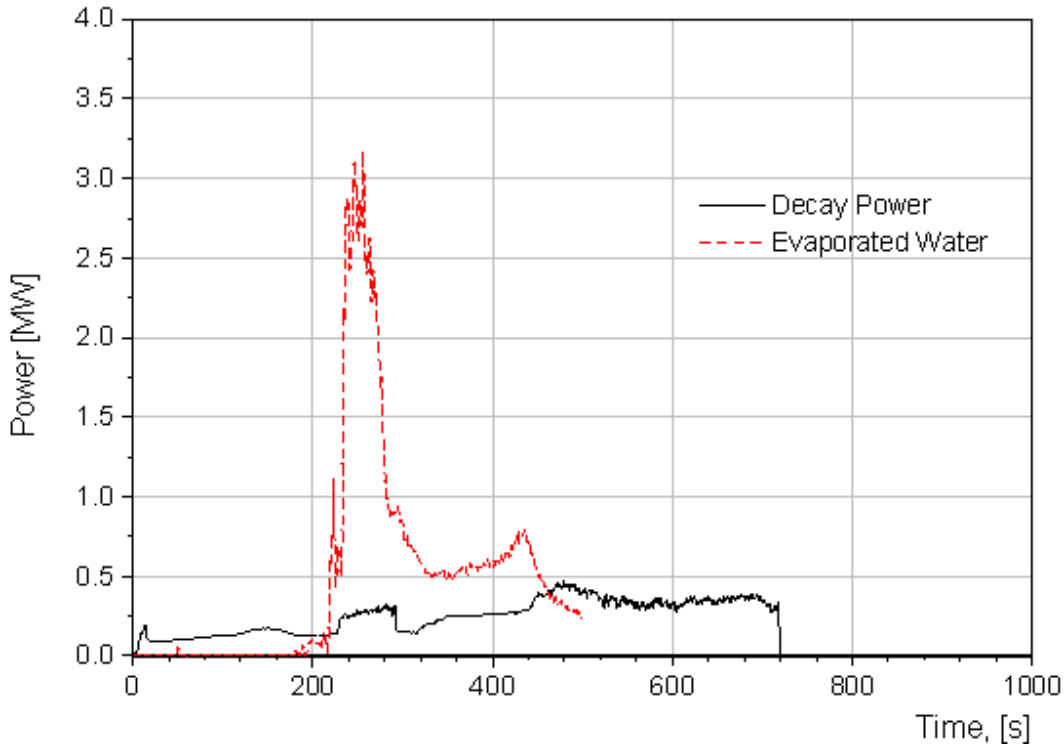

Figure 12: Comparison of decay power and power extracted by evaporation

Comparison of off-gas and decay power is given in Fig. 12. This plot underlines the initially high cooling rate, and shows that the steam rate approaches the decay heat thereafter.

The high, but only short early cooling peak is certainly not sufficient to quench the complete melt. In agreement with the video observations, this is the period where crust formation on top and bottom of the melt takes place. The fast drop of the extracted power indicates that removal of the energy from the bulk of the melt in the present test is not very effective and needs considerably more time than in previous experiments. Indeed, post test sectioning of the crucible shows only small porosity of the solidified melt, which is responsible for the long lasting heat extraction from the bulk of the melt.

3.2.4 Gas Release

This section describes the gas flow during the test, measured in the hood of the crucible and in the off-gas line, which connects the crucible with the open atmosphere.

The gas pressure in the hood is given in Fig. 13, showing a practically constant atmospheric pressure. Some very small oscillations are detected after 220 s when passive bottom flooding starts. In spite of direct contact of water and melt, no significant pressure spikes do occur. This is a consequence of the controlled water injection through the porous concrete layer, which brings in the water in small portions only and excludes energetic pressure spikes.

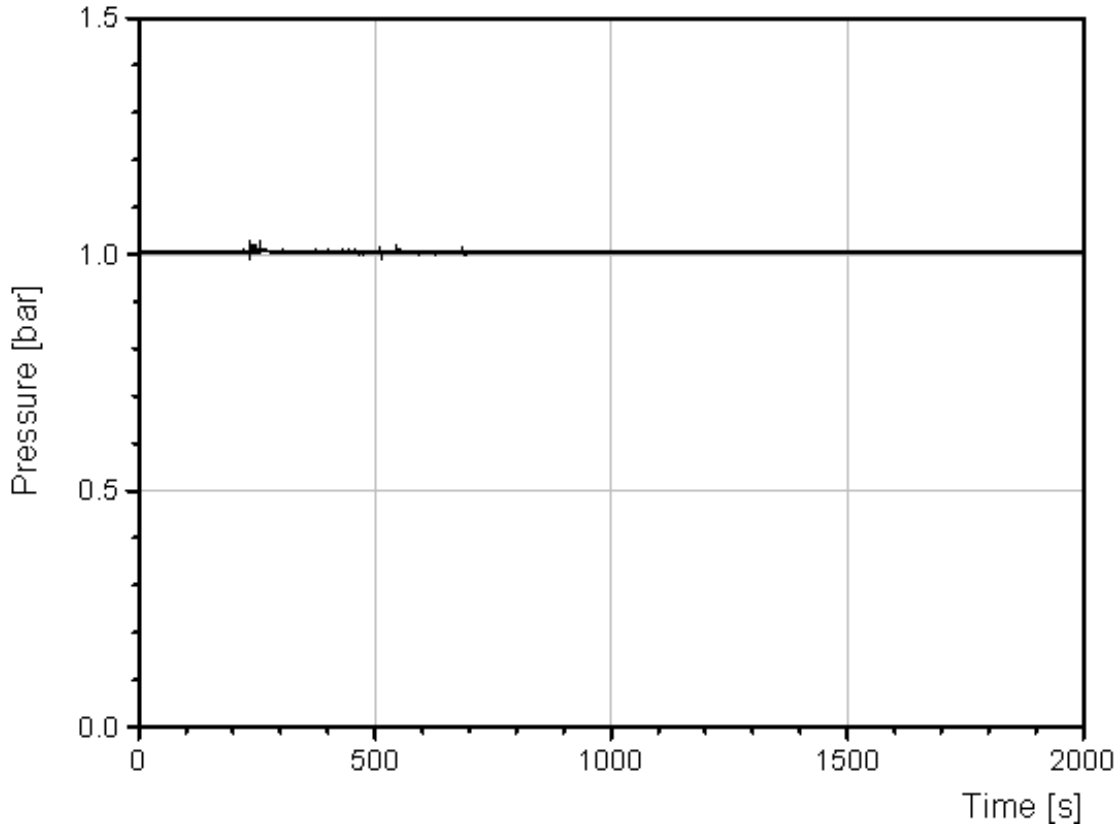

Figure 13: Gas pressure in the hood of the crucible

The off-gas temperature in the crucible hood is given in Fig. 14, measured by a thermocouple protruding into the gas volume. This temperature is used to determine the enthalpy of the steam flow after onset of bottom flooding as discussed in section 3.2.3.

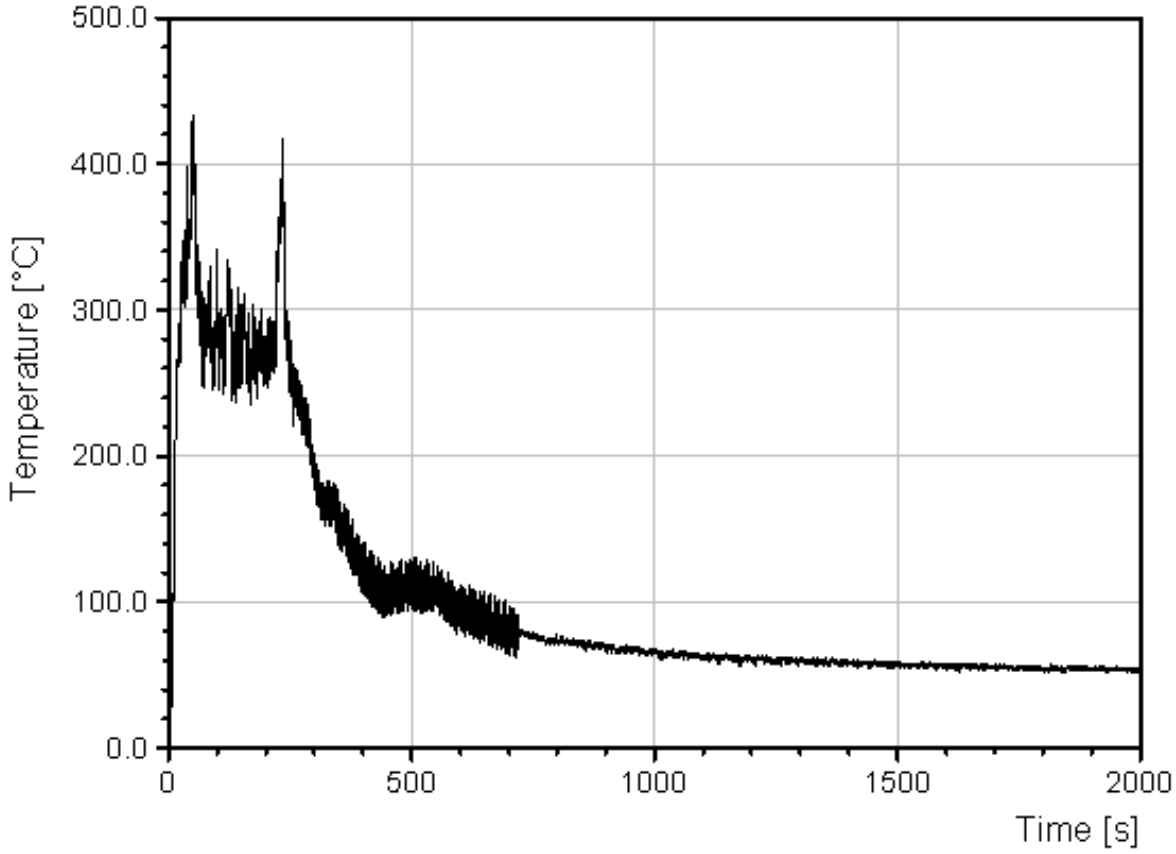

Figure 14: Gas temperature in the hood of the crucible

When the melt is poured into the crucible, the off-gas temperature rises up to 400°C, and then reduces to about 300°C during ongoing dry concrete erosion. It is evident, that the gases deposit part of their energy to the cold structures of the upper crucible. With onset of bottom flooding at 220 s and the massive steam flow, the gas temperature rises up again to about 400°C. This high steam flow results in a peak gas flow in the off-gas line of 18 m/s, lasting only some 50 s. The gas temperature rapidly reduces and reaches about 100°C at 400 s. As the melt at this time is completely covered by a growing water layer, the steam released from the melt surface is close to saturation. After 500 s the gas temperature in the hood falls below 100°C, and boiling of the water layer on top of the encrusted melt reduces continuously. Therefore, some condensation may occur in the crucible hood.

Gas composition was measured online by a quadrupole mass spectrometer that detects up to 8 chemical species. Fig. 15 shows the results for the gases H_2, CH_4, CO, and CO_2. The steam content could not be detected because of principal limitations of the measurement system: As steam would damage the analysis system, steam flow in the analysis system was removed by condensation. The constant argon cover gas flow is not shown in Fig. 15, but was used as the reference to determine the release rates of the species based on their measured concentration.

The mass spectrometer was calibrated before and after the test with 5 test gases of different compositions. The release rates are given in litre/s at standard gas conditions: 1 l/s corresponds to 1/22.4 mole/s. Note, that due to the long response time of the gas analysis system, the time axis for the gas rates should be shifted by about 30 s to the left side.

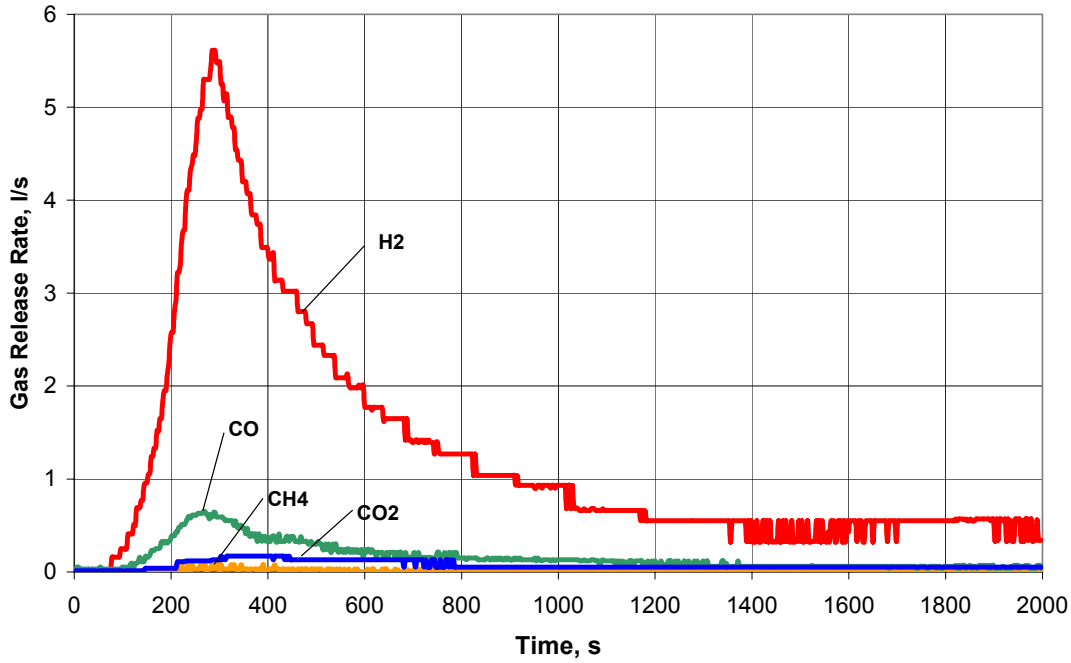

Figure 15: Release rates of H_2, CH_4, CO, and CO_2 in the off-gas

The most interesting and most important gas is hydrogen, which is formed by oxidation of metal through steam. Measurements show an increase of the hydrogen release rate, which reaches a peak value of 5.5 l/s at onset of bottom flooding. The increase of hydrogen production with flooding is as expected. Unexpected and not explained is the lack of a pronounced hydrogen peak during the first phase of dry concrete erosion, which in former experiments generated a peak of similar height. This lack of measured hydrogen is in agreement with a non-existing flame at the end of the off-gas line. The decrease of the hydrogen rate after 300 s indicates the drop of the metal temperature through the cooling process, which reduces the velocity of the chemical reaction. Although the hydrogen rate goes down continuously, it is still above zero at 720 s, when decay heating is terminated. This is an indication, that parts of the metal phase still have an elevated temperature, or may be not yet completely solidified. After 1200 s the hydrogen rate has a constant low “offset” value, which corresponds to zero release.

CO and CO_2 are gases, which form during concrete decomposition from carbonates that are present in small quantities in the concrete, and by the subsequent reaction with the metal melt, respectively. Their concentration is negligible after onset of cooling, because concrete erosion comes to an end. CH_4 may form by further gas reactions and would be important as potential reaction partner to form organic iodine. No significant amount of methane is however detected.

Figure 16 gives the integrated gas release as determined by integration of Fig.15. Some 2000 l of hydrogen are generated during the cooling process.

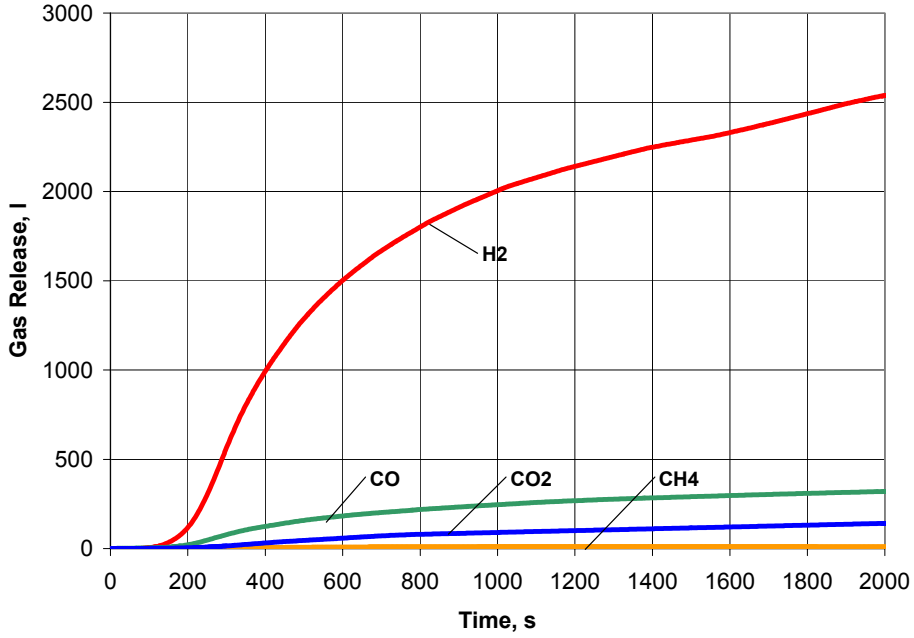

Figure 16: Integrated gas release rates of H_2, CH_4, CO, and CO_2 in the off-gas

The aerosol concentration was measured by the absorption of a laser beam that passes the off-gas line. The extinction E is defined by the logarithmic ratio of the intensity I/I_0 of the laser beam before and after transmission through the off-gas tube

$$E = \ln (I/I_0)$$

and is in the present application a qualitative information of the aerosol density. Figure 17 shows from 0 to 220 s aerosol release during the phase of dry concrete erosion. With onset of bottom flooding the aerosol density is drastically reduced. The low-density aerosol, still detected in the period from 400 to 600 s, may be attributed to the volcanic eruptions. Afterwards, the aerosol concentration is practically zero.

The reduction of the aerosol production with onset of bottom flooding has 3 reasons:

1. Stop of concrete erosion ends the release of aerosols from decomposing concrete.
2. The surface crust of the melt stops evaporation from the hot melt.
3. The water layer on top of the melt traps aerosol particles.

Figure 17 shows that bottom flooding is very effective to reduce aerosols and fission products, which may be present in the form of aerosol particles, and that aerosol release is limited to the short period of dry concrete erosion.

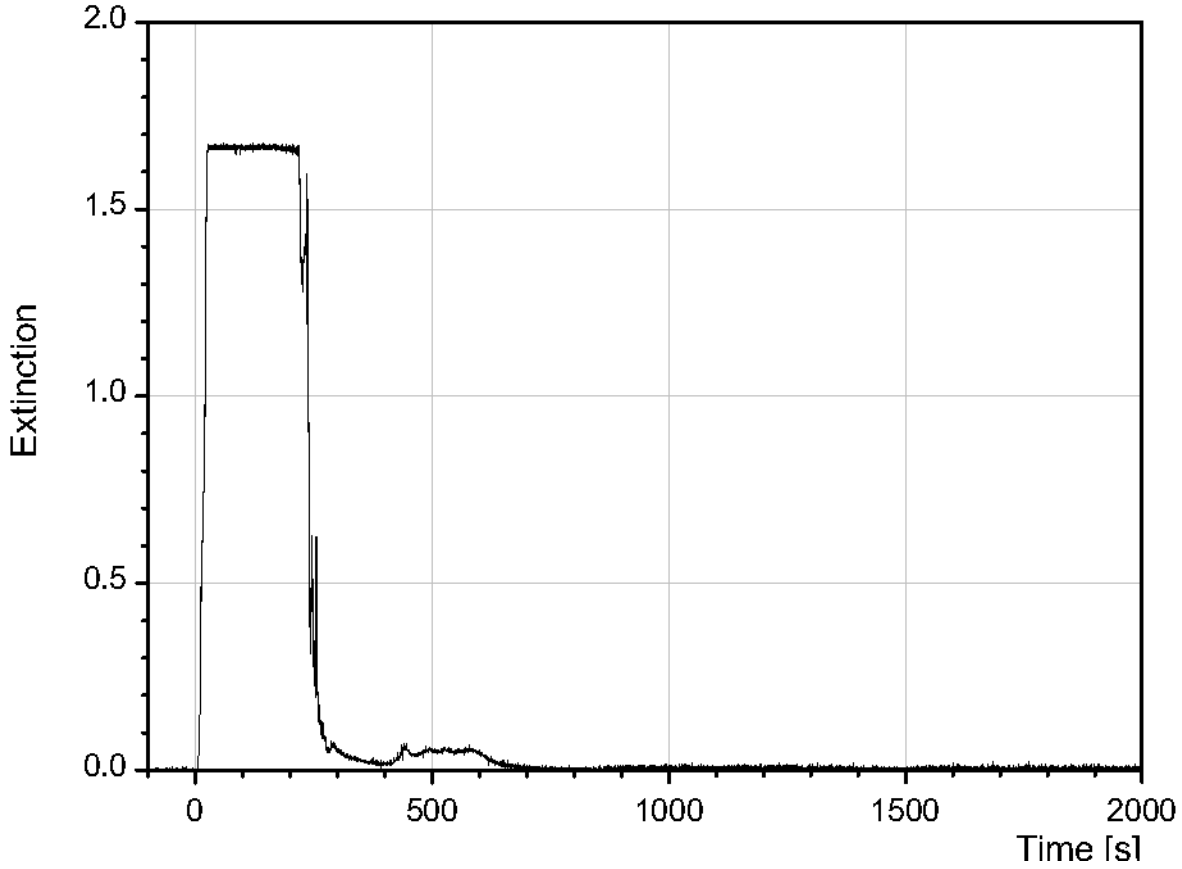

Figure 17: Extinction of laser beam by aerosols in the off-gas line

3.2.5 Concrete Erosion

The erosion of the sacrificial concrete layer was determined from the failure time of a series of thermocouples, which were located in the centreline of the coolant device and in the middle of the 4 quadrants, named NW, SW, SE, and NE, respectively. The position of the thermocouples referred to the upper surface of the porous concrete layer (0 mm), is + 8, + 18, + 28, and + 38 mm, respectively. The top of the sacrificial layer corresponds to +50 mm.

Fig. 18 shows the front position versus time over the period from 0 to 800 s. At 10 s, the erosion starts at the upper surface (+50 mm) and reaches the + 18 mm level at about 200 s. The erosion as detected by the thermocouples is relatively even. Deviations from a flat surface are 7 mm, which corresponds to about 40 s erosion time. The average erosion velocity over this period is 0.17 mm/s, to be attributed to the erosion by the metal phase. No significant decrease of the erosion velocity with time is observed. This is in agreement with previous tests, including the BETA experiments, which showed no major variations of the erosion rates, as long as the metal melt is above liquidus.

Flooding is expected when the melt reaches the + 6 mm position, which is defined by the upper surface of the ceramic tiles, which then would fail by cracking and allow the water inflow. Extrapolation with the average erosion velocity would yield start of flooding at 260 s. Actually, flooding starts at 220 s, which may be initiated by a part of the melt, which is preceding the detected average melt position. The onset of cooling

delays and stops further erosion. Thermocouples at the +8 mm position fail at 740 s only or remain intact. This is described by the flat erosion line in Fig. 18.

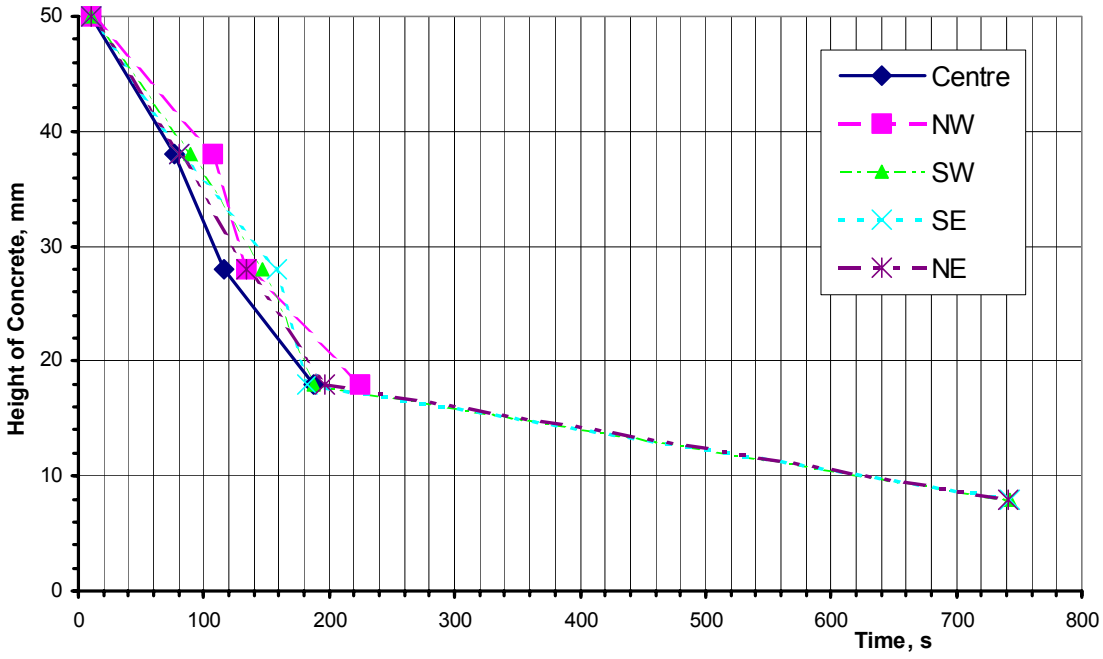

Figure 18: Erosion front of melt in sacrificial concrete from thermocuple measurements

3.3 Post Test Analysis

The apparatus was carefully disassembled in order to document the debris configuration with respect to coolability. Only very little (some 2 kg) loose oxide material was removed from the upper melt surface. This material may be fallen down from the upper crucible surface or may be generated by volcanic eruptions. A significant layer of oxide material was deposited at the sidewalls of the crucible, generated during the first phase of vigorous dry MCCI and at onset of bottom flooding.

Figure 19 is a photograph of the oxide melt surface, which fills the lower of the 3 ceramic rings, 40 cm high. The photograph shows a rough surface which formed during the early process of bottom flooding and which solidified when the coolant water covered the upper surface at about 300 s. Above this relatively horizontal surface, a pronounced volcanic eruption rises some 25 cm high, in the northeast section of the surface (Fig. 20). The irregular dome consists of pure oxide material that welded together and formed the pile during the period of volcanic eruptions from 360 s to 510 s. At the base of the dome, a dense lava flow covers the rough crust, which was formed before. In general, the dome has a dense structure, with low porosity. But some cavities exist, which however have no connection to some flow path below and are not permeable for water, as was tested by pouring water on the upper surface. Evidently, the volcanic eruption ended by blockage of the main flow path to the tip of the dome. In summary, the eruption, although driven by a large

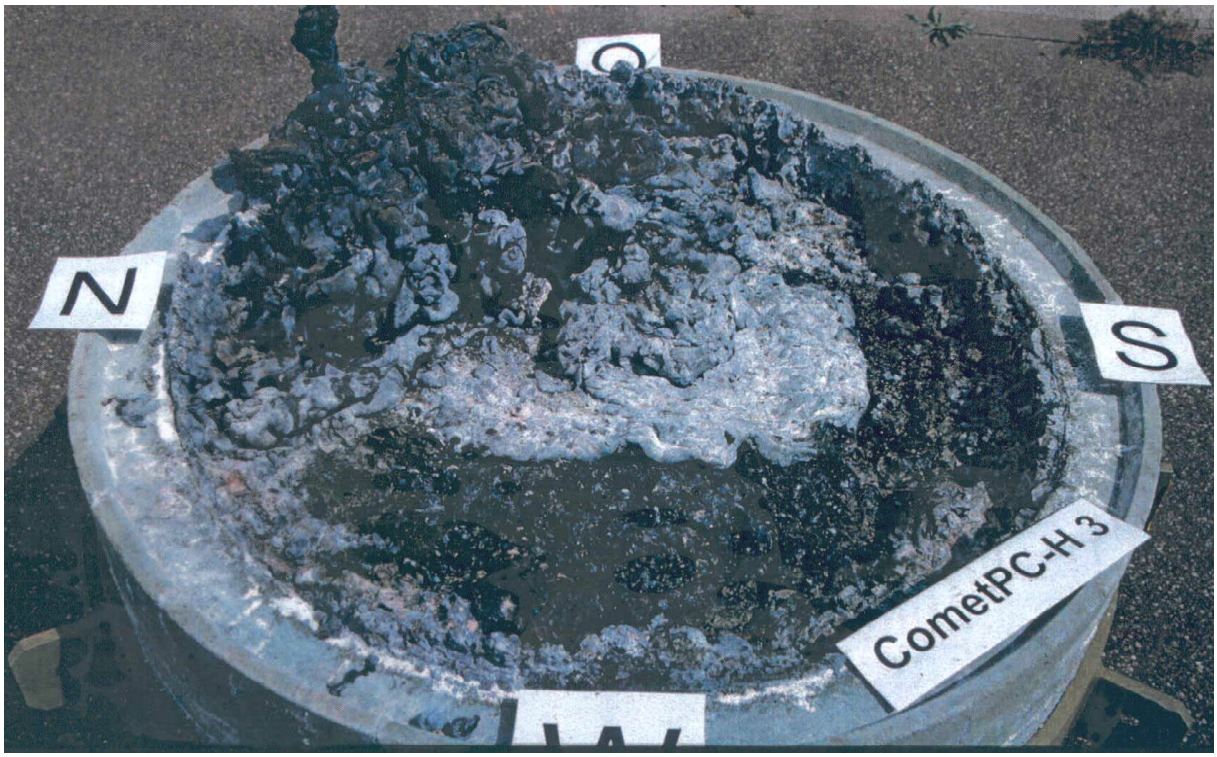

Figure 19: Surface of the solidified oxide melt with volcano formed in northeast

Figure 20: Closeup view of the volcanic eruption in northeast

steam flow from the bottom injected water, did not contribute significantly to coolability, as neither a loose particle bed nor a permeable dome structure was created. This is a remarkable difference from some of the MACE tests, which were performed at ANL, and which produced some loose particle bed from parts of the melt. It is supposed, that the type of volcanism depends on the silica content in the melt and is influenced by the viscosity.

There is only one dominant flow channel, which allows steam and water flow through the solidified melt. This is illustrated in Fig. 21, which is a section through the debris in the direction northeast to southwest, that is through the centre of the dome and the flow channel. The flow channel with a diameter of about 20 mm in the upper surface, is located at the base of the dome some 18 cm northeast of the centre of the surface, and extends downwards through the oxide melt to the metal layer at the bottom. No other major flow path is detected.

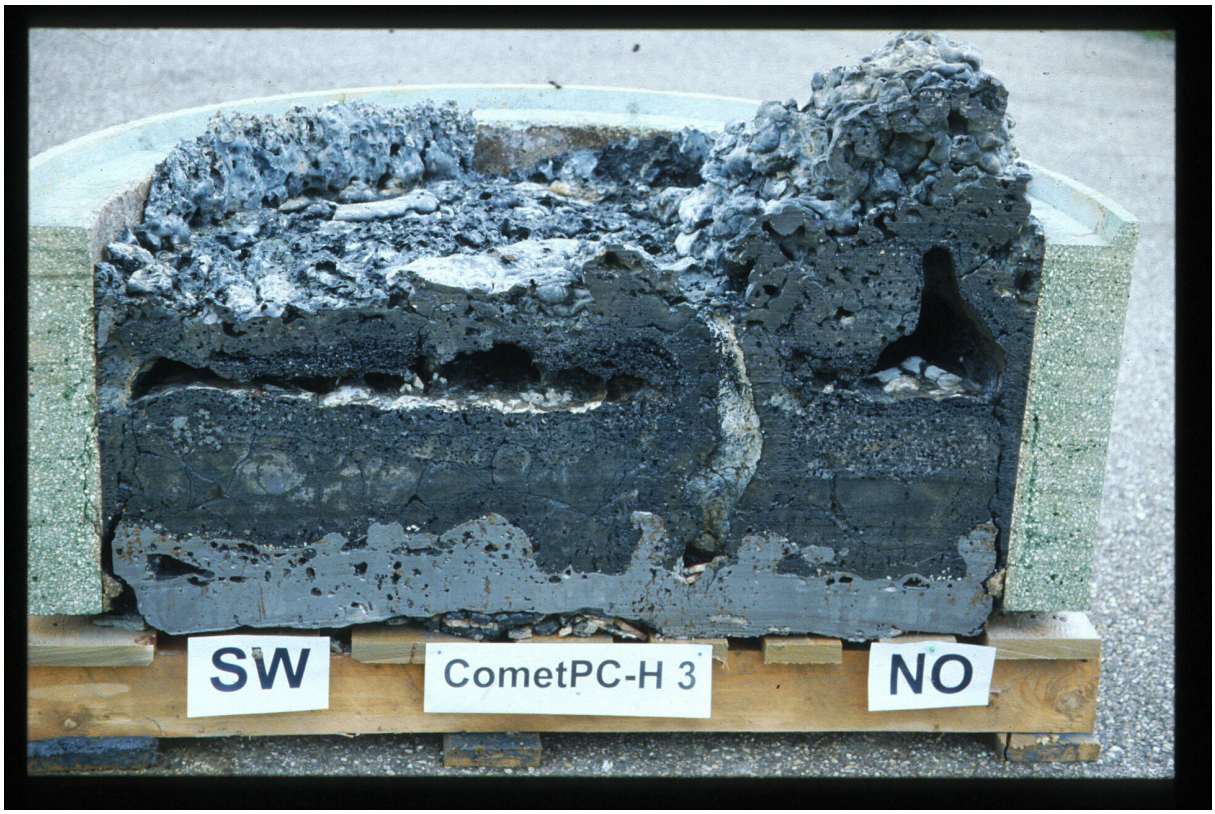

Figure 21: Solidified melt, sectioned through the volcanic cone, direction SW to NE

The sectioned debris shows 3 layers of low porosity:

1. The steel layer at the bottom, 5 to 10 cm high.
2. An intermediate oxide layer, 15 to 20 cm thick.
3. The upper oxide layer, 5 to 8 cm thick with the volcanic dome on the NE side.

The two oxide layers are separated by a large flat cavity, which extends nearly over the complete surface of 92 cm. The height of this cavity is 2 to 6 cm, and 15 cm in the dome. The coolant flow channel has formed a hollow cylinder of oxide material, which connects layers 2 and 3, bridging the cavity. The lower surface of the cavity is completely flat, indicating the free surface of a collapsed melt that at some time

during the test separated from the upper crust, which formed and stabilized when the melt was flooded by the coolant water. The low porosity especially of the intermediate oxide layer indicates, that later in the test all steam/water flow passed through the dominant flow channel, and no steam flow was maintained through the bulk of the oxide melt. This allowed the still liquid fraction of the oxide melt to collapse, to separate from the upper crust, and to form the surface of a flat internal pool, which solidified after end of decay heating. A closer view of the intermediate oxide layer in Fig. 21 shows a dense agglomerate of many melt particles in the oxide layer. The particles are about 5 cm in size and are present all over the sectioned diameter. They are products of the early fragmentation process and formed during the first period of bottom flooding. Cooled by the steam/water flow, these fragments started to solidify, forming a growing particle crust. But when the steam/water flow concentrated to the dominant flow channel, the particles and the remaining liquid melt collapsed, forming the dense intermediate layer in Fig. 21.

The low porosity of the three layers is unexpected and does not correspond to the fragmentation processes, which are expected as a result of the bottom flooding process. The low porosity is certainly not sufficient to remove the decay heat from the bulk of the melt, and therefore a significant fraction of the (oxide) melt did not solidify during the heated phase of the test. This resulted in the following situation at the end of the heated test phase:

The majority of the metal phase at the bottom is cooled and solidified (mostly below the Curie temperature of 400°C) by the coolant water flow in the porous concrete layer underneath. The heat in the metal crust is removed by the steam/water flow from the porous concrete layer to the upper surface through the dominant flow channel. From the upper crust, the heat is transferred by boiling to the upper water layer. The oxide melt, safely enclosed between top und bottom crusts, however, remains liquid. This situation is stable as long as the decay heat can safely be removed, without attack especially of the lower structures.

Fig. 22 is a photograph of the upper porous concrete layer taken from above, after removal of the solidified melt. The ceramic tiles which cover 70 % of the porous concrete layer, are clearly visible (compare the schematic design in Fig. 1). Some of the tiles were removed with the solidified melt. As the tiles have no tight connection to the lower concrete, they allow the passage of water and steam to the free surface mainly in the northeast section. In this section, where the volcano was located, the ceramic tiles were first contacted and destroyed by the melt, which initiated the coolant water flow.

Fig. 23 is a section through the porous concrete layer and the supporting concrete structure in the same direction as the solidified melt was cut. The left part corresponds to the northeast sector, where the melt to some degree attacked the water filled porous concrete layer, while the southwest sector was completely intact (only partially reproduced in Fig. 23). The total height of the porous concrete layer is 100 mm. The upper porous concrete in a 25 cm diameter area in northeast (visible in Fig. 22) is slightly attacked about 25 mm deep: The upper 5 mm concrete surface has formed a glassy structure. The concrete below to - 25 mm lost some of its strength as the cement was destroyed by the elevated temperature. Underneath, the remaining 75 mm of porous concrete are completely intact as always cooled by the presence of the flooding water. This identifies the water filled, porous concrete layer

as a robust safety barrier, which is able to stop and stabilize the melt even if some attack should occur. – The sidewalls in Fig. 23 made of standard structural concrete, are completely intact as cooling in this area was also very efficient.

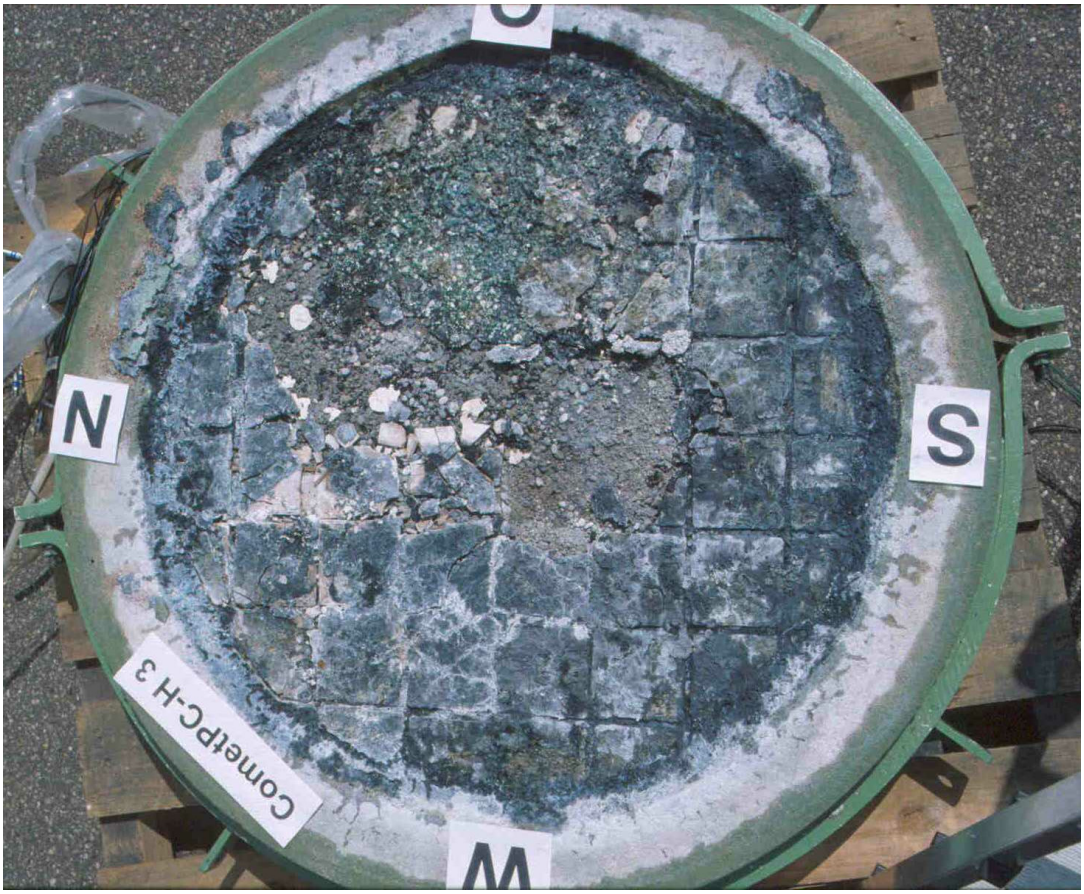

Figure 22: Surface of the upper porous concrete layer after removal of the solidified melt

Figure 23: Porous concrete layer after test, sectioned in direction NE to SW

4. Conclusions

The experiment with 800 kg oxide + metal melt and decay heat simulation has shown the following phenomena during the cooling process:

1. Dry, relatively even erosion of the upper sacrificial concrete layer with an erosion velocity of 0.17 mm/s by the metal melt.
2. Passive onset of bottom flooding with some 2 litres water/(m^2·s) after 220 s only, according to the low height of the sacrificial concrete layer. Strong agitation of the melt with high steam release through evaporating water indicates the high efficacy of bulk cooling. Initial cooling rate is about 4 MW/m^2.
3. Fast formation of a porous surface crust and continuous flooding of the crust by water from the bottom (about 300 s). The bulk of the melt under the crust is, however, still liquid.
4. Downward propagation of the melt stops near the surface of the porous, water filled concrete layer.
5. During a certain period, steam/gas flow from bottom flooding leads to volcanic eruptions in the northeast sector of the surface. Outflow of steam concentrates to the volcanic centre, with the consequence that the majority of the remaining surface crusts becomes impermeable. The eruptions pile up an irregular volcanic dome of low porosity oxide melt, but only minor particle bed (if any) is formed. Therefore, the contribution of volcanism to coolability is small.
6. Volcanism ends after 510 s. All steam/water flow from bottom flooding concentrates to one dominant hole at the bottom of the dome without further melt ejection. The remaining liquid melt, which is enclosed between top and bottom crusts, collapses and separates from the surface crust. This creates a flat cavity between melt and upper surface crust.
7. Stable situation reached after about 700 s: Melt stabilized by porous water filled concrete layer. Solid crust of low porosity only formed at bottom and top of the melt. Residual liquid melt enclosed between bottom crust and voided cavity. Heat removal from top and bottom crusts corresponds to simulated decay heat.
8. Unfortunately, an erroneous control signal switched off the decay heat simulation and did not allow further observation of the long-term cooling processes.
9. All cooling processes were “mild” in the sense that no energetic processes or pressure spikes did occur when water was added to the bottom of the melt.

The final configuration of the melt, although stable with respect to heat removal and stop of concrete erosion, did not correspond to the expected porously solidified melt that was observed in previous experiments. In the present experiment, one dominant flow channel developed later in the test, through which most of the coolant steam/water flow passed the melt. Consequently, a significant part of the bulk of the oxide melt, as not in direct contact with the coolant flow, remained liquid, enclosed between top and bottom crusts. This situation is stable as long as the decay heat can safely be removed through the crusts. In the actual experiment this was provided by the robustness of the water filled porous concrete layer under the melt, and the water covering the melt surface.

The reason for the lack of porosity in comparison with previous tests may be the small height of the sacrificial concrete layer, which with regard to better inductive heating of the melt after repair of the induction coil, was reduced from 10 to 20 cm typical to 5 cm only. This results in less silica content in the oxide melt and a higher temperature with the consequence of a lower viscosity of the melt at onset of bottom flooding. The consequence is a delayed formation of the porosity because of fast collapse of the void in a low viscosity melt.

In summary, the experiment has demonstrated that the CometPC cooling concept is able to stop and to cool the melt, although the expected porosity formation of the majority of the melt did not occur. Under this aspect, the porous concrete layer has proven its reliability to stop the melt. On the other side, volcanic melt eruptions which occurred during a limited period of the test, did not improve the coolability significantly, as no major new porosity was created.

Following the principle idea of the COMET concept, the coolability of the melt by porosity formation remains an important issue to be strengthened. Further tests shall investigate the homogeneity of the fragmentation and cooling process and its improvement, as well as the long-term stability of the cooling process.